PROCEEDINGS A

rspa.royalsocietypublishing.org

Research

Cite this article: Hutchinson JW. 2016 Buckling of spherical shells revisited. *Proc. R. Soc. A* **472**: 20160577.
http://dx.doi.org/10.1098/rspa.2016.0577

Received: 20 July 2016
Accepted: 13 October 2016

Subject Areas:
mechanical engineering, mechanics

Keywords:
buckling, bifurcation, spherical shells, geometric imperfections

Author for correspondence:
John W. Hutchinson
e-mail: jhutchin@fas.harvard.edu

Buckling of spherical shells revisited

John W. Hutchinson

School of Engineering and Applied Sciences, Harvard University, Cambridge, MA 02138, USA

JWH, 0000-0001-6435-3612

A study is presented of the post-buckling behaviour and imperfection sensitivity of complete spherical shells subject to uniform external pressure. The study builds on and extends the major contribution to spherical shell buckling by Koiter in the 1960s. Numerical results are presented for the axisymmetric large deflection behaviour of perfect spheres followed by an extensive analysis of the role axisymmetric imperfections play in reducing the buckling pressure. Several types of middle surface imperfections are considered including dimple-shaped undulations and sinusoidal-shaped equatorial undulations. Buckling occurs either as the attainment of a maximum pressure in the axisymmetric state or as a non-axisymmetric bifurcation from the axisymmetric state. Several new findings emerge: the abrupt mode localization that occurs immediately after the onset of buckling, the existence of an apparent lower limit to the buckling pressure for realistically large imperfections, and comparable reductions of the buckling pressure for dimple and sinusoidal equatorial imperfections.

1. Introduction

The intense study of the nonlinear buckling behaviour of shells and, in particular, of spherical shells largely ended almost five decades ago with the publication of Koiter's [1] monumental paper on the post-buckling behaviour and imperfection sensitivity of spherical shells subject to external pressure. Spherical shells under external pressure and cylindrical shells under axial compression display extraordinarily nonlinear post-buckling behaviour with a sudden loss of load-carrying capacity triggered by buckling. These two shell/loading combinations are the most imperfection sensitive in the sense that experimentally measured buckling loads are often as little as 20% of the buckling load predicted for the perfect structure. As a consequence, design codes for

THE ROYAL SOCIETY PUBLISHING

elastic buckling of these thin shell structures often stipulate that the design load is 'knocked down' to 20% of that of the buckling load of the perfect structure. This empirical rule was proposed over 50 years ago based on a large body of collected experimental buckling data and is still the governing design rule.

No attempt will be made here to survey the prior extensive literature on spherical shell buckling. Nevertheless, related to present aims, it should be mentioned that the highly nonlinear character of spherical shell buckling was appreciated in the first half of the 1900s and an important step in coming to terms with the nonlinearity and strong imperfection sensitivity was taken by von Karman & Tsien [2], who set in motion a quest for a quantitative criterion governing the low buckling loads of thin spherical and cylindrical shells. A large literature addressing this topic accrued over the next 30 years investigating criteria such as a minimum post-buckling load or a load at which the energy in the buckled state equals that in the unbuckled state. So far, no acceptable criterion of this type based on the response of the perfect shell has emerged. Instead, more progress has resulted from the consideration of initial imperfections and their role in reducing the buckling load, although progress along these lines for spherical shells was limited, as will be described in this paper. Koiter [3] developed a general theory of elastic stability which connected imperfection sensitivity to the initial post-buckling behaviour of the perfect structure. Relevant to the present study, it must be noted that a limitation of the Koiter theory is that the imperfection-sensitivity predictions are asymptotic and only valid for sufficiently small imperfections. The range of validity is not known from the theory itself and varies from problem to problem. Spherical shell buckling is particularly challenging in this regard because the direct application of Koiter-type theory to full spheres under external pressure, first presented by Thompson [4] and somewhat later by Koiter [1], turns out to be valid for only extremely small imperfections, too small to be representative of those in actual shells. This paper brings out clearly the reason underlying the small range of validity of the Koiter theory for full spherical shells and presents accurate buckling pressure results for representative imperfection amplitudes and shapes.

The lull in research on spherical shell bucking over the past several decades has been superseded by a resurgence of activity driven from several quarters. Recent advances with soft elastomeric materials have made it possible to fabricate spherical shells that either are near perfect or have precisely controlled imperfections, thereby opening the way for systematic experimental imperfection-sensitivity studies [5,6]. These laboratory developments align with efforts underway at NASA and by others interested in large shell structures to replace the long-standing empirical buckling knock-down factors employed in design codes with an approach that computes buckling loads using commercial finite-element codes by incorporating realistic imperfections tied to manufacturing processes and direct measurement. Spherical shell buckling has also attracted interest for applications as diverse as pattern formation and in the life sciences in the study of capsules, pollen grains and viruses [7–11]. From a mathematical perspective, spherical and cylindrical shells are interesting because of their complicated bifurcation behaviour and their highly unstable post-buckling response. Recent work in the nonlinear dynamics community has focused on these structures with the aim of gaining both a qualitative understanding of the nonlinear system and a quantitative understanding of what sets the apparent lower limit of the buckling loads [12–14].

2. Three shell theories

Three nonlinear shell theories for analysing buckling of spherical shells will be employed in this paper. The rationale for doing so is to establish the range of applicability of the two most commonly used sets of nonlinear buckling equations—small strain–moderate rotation theory and Donnell–Mushtari–Vlasov (DMV) theory—in application to spherical shell buckling. A theory which employs exact stretching and bending strain measures for the middle surface of the perfect shell undergoing axisymmetric buckling deformations will be used to benchmark the

two commonly used theories. Most of the results in this paper are computed with small strain–moderate rotation theory, but DMV theory is also used to carry out the classical bifurcation analysis and discussed throughout because of its widespread use in the analysis of spherical shell buckling. All three theories are the so-called first-order theories intended for application to thin shells. Such theories provide an accurate representation of the energy in stretching and bending in the constitutive model to first order in t/R with t as the shell thickness and R as its radius. Moderate rotation theory will be specified first, followed by DMV theory and finally the exact theory.

(a) Small strain–moderate rotation theory

For the all problems of interest here, the middle surface strains remain small. In addition, for all but an initial set of examples, the rotations remain moderately small. In nonlinear shell theory, this means that middle surface strains ε satisfy $|\varepsilon| \ll 1$ and rotations φ about the middle surface tangents and normal satisfy $\varphi^2 \ll 1$. As a rough rule of thumb, the rotations should not exceed about 15–20° for this theory to remain accurate. Rotations about the middle surface tangents are the largest while the rotation about the normal to the shell middle surface will turn out to be very small in the sphere buckling problem. Nevertheless, the equations accommodate moderate rotations about the normal. Our calculations will also show that there is almost no difference between dead pressure (force per original area acting in the original radial direction) and live pressure (force per current area acting normal to the deformed middle surface) for the behaviour of interest in this paper, but both loadings will be modelled to establish this fact. It should be noted that, in this paper, dead pressure does not imply that the pressure is prescribed to be fixed, as the terminology 'dead' sometimes implies. In this paper, 'prescribed pressure' will be the terminology used to characterize a loading condition in which p is held constant whether the pressure is dead or live. Equations for a first-order shell theory with small strains and moderate rotations were given by Sanders [15], Koiter [16,17] and Budiansky [18]. These are specialized below for initially perfect spherical shells followed by the introduction of small initial geometric imperfections.

Euler coordinates (ω, θ, r) are employed with r as the distance from the origin, ω as the circumferential angle and θ as the meridional angle ranging from 0 at the equator to $\pi/2$ at the upper pole. The radius of the undeformed middle surface of the shell is R. A material point at (ω, θ, R) on the middle surface of the undeformed shell is located on the deformed shell at

$$\bar{\boldsymbol{r}} = u_\omega \boldsymbol{i}_\omega + u_\theta \boldsymbol{i}_\theta + (R + w)\, \boldsymbol{i}_r, \tag{2.1}$$

where $(\boldsymbol{i}_\omega, \boldsymbol{i}_\theta, \boldsymbol{i}_r)$ are unit vectors tangent and normal to the undeformed middle surface associated with the respective coordinates. For general deflections, the displacements (u_ω, u_θ, w) are functions of ω and θ; for axisymmetric deflections $u_\omega = 0$, while the other two displacements are functions only of θ.

The nonlinear strain–displacement relations make use of the linearized middle surface strains $(e_{\omega\omega}, e_{\theta\theta}, e_{\omega\theta})$ and the linearized rotations $(\varphi_\omega, \varphi_\theta, \varphi_r)$ with the rotation components about $\boldsymbol{i}_\theta$, $\boldsymbol{i}_\omega$ and $\boldsymbol{i}_r$, respectively, which are

$$\left.\begin{aligned} e_{\omega\omega} &= \frac{1}{R}\left(\frac{1}{\cos\theta}\frac{\partial u_\omega}{\partial \omega} - \tan\theta\, u_\theta + w\right), \\ e_{\theta\theta} &= \frac{1}{R}\left(\frac{\partial u_\theta}{\partial \theta} + w\right) \\ \text{and} \quad e_{\omega\theta} &= \frac{1}{2R}\left(\frac{\partial u_\omega}{\partial \theta} + \frac{1}{\cos\theta}\frac{\partial u_\theta}{\partial \omega} + \tan\theta\, u_\omega\right) \end{aligned}\right\} \tag{2.2}$$

and

$$\left.\begin{aligned}\varphi_\omega &= \frac{1}{R}\left(-\frac{1}{\cos\theta}\frac{\partial w}{\partial \omega}+u_\omega\right),\\ \varphi_\theta &= \frac{1}{R}\left(-\frac{\partial w}{\partial \theta}+u_\theta\right)\\ \text{and}\quad \varphi_r &= \frac{1}{2R}\left(\frac{1}{\cos\theta}\frac{\partial u_\theta}{\partial \omega}+\tan\theta\, u_\omega-\frac{\partial u_\omega}{\partial \theta}\right)\end{aligned}\right\} \tag{2.3}$$

In the small strain–moderate rotation theory, the middle surface strains are nonlinear

$$\left.\begin{aligned}E_{\omega\omega} &= e_{\omega\omega}+\frac{1}{2}\varphi_\omega^2+\frac{1}{2}\varphi_r^2,\\ E_{\theta\theta} &= e_{\theta\theta}+\frac{1}{2}\varphi_\theta^2+\frac{1}{2}\varphi_r^2\\ \text{and}\quad E_{\omega\theta} &= e_{\xi\theta}+\frac{1}{2}\varphi_\omega\varphi_\theta,\end{aligned}\right\} \tag{2.4}$$

while the bending strains are linear

$$\left.\begin{aligned}K_{\omega\omega} &= \frac{1}{R}\left(\frac{\partial \varphi_\omega}{\partial \omega}-\tan\theta\,\varphi_\theta\right),\\ K_{\theta\theta} &= \frac{1}{R}\frac{\partial \varphi_\theta}{\partial \theta}\\ \text{and}\quad K_{\omega\theta} &= \frac{1}{2R}\left(\frac{\partial \varphi_\omega}{\partial \theta}+\frac{1}{\cos\theta}\frac{\partial \varphi_\theta}{\partial \omega}+\tan\theta\,\varphi_\omega\right).\end{aligned}\right\} \tag{2.5}$$

In this paper, imperfections in the form of a small, initial, stress-free radial deflection of the middle surface w_{I} from the perfect spherical shape are considered with $(u_\omega, u_\theta)_{\mathrm{I}}=0$. Imperfections in the form of thickness variations or residual stresses will not be considered. Thickness variations can give rise to both non-uniform pre-buckling stresses and initial middle surface undulations but in most structures thickness variations are controlled to a much high tolerance than middle surface undulations. In addition, in this paper attention is limited to *axisymmetric imperfections* such that w_{I} is a function of θ but not ω. Assuming that w_{I} itself produces small middle surface strains and moderate rotations (a condition always met in all our examples), denote the strains in (2.4) arising from w_{I} by $E^I_{\alpha\beta}$. Then, evaluate the total strains due to $(u_\omega, u_\theta, w_{\mathrm{I}}+w)$, where w is additional to w_{I}, and denote the result by $E^{I+U}_{\alpha\beta}$. The strains arising from displacements additional to w_{I}, which produce the stresses, are $E_{\alpha\beta}=E^{I+U}_{\varepsilon\beta}-E^I_{\alpha\beta}$ and these are given by

$$\left.\begin{aligned}E_{\omega\omega} &= e_{\omega\omega}+\frac{1}{2}\varphi_\omega^2+\frac{1}{2}\varphi_r^2,\\ E_{\theta\theta} &= e_{\theta\theta}+\frac{1}{2}\varphi_\theta^2+\frac{1}{2}\varphi_r^2-\frac{1}{R}\frac{\mathrm{d}w_{\mathrm{I}}}{\mathrm{d}\theta}\varphi_\theta\\ \text{and}\quad E_{\omega\theta} &= e_{\xi\theta}+\frac{1}{2}\varphi_\omega\varphi_\theta-\frac{1}{2R}\frac{\mathrm{d}w_{\mathrm{I}}}{\mathrm{d}\theta}\varphi_\omega,\end{aligned}\right\} \tag{2.6}$$

where the linearized strains and rotations are evaluated in terms of $(u_\omega,\ u_\theta,\ w)$. Because the bending strains are linear in the displacements and their gradients, the same process reveals that the relations (2.5) still hold for the relationship between the bending strains and the additional displacements with no influence of w_{I}. From this point on, the additional displacements $(u_\omega,\ u_\theta,\ w)$ will simply be referred to as the displacements. An imperfection contribution also arises for live pressure loading which will be introduced shortly.

The stress–strain relations for a shell of isotropic material in each of the three first-order theories employed here are

$$\left.\begin{aligned}N_{\alpha\beta} &= \frac{Et}{(1-\nu^2)}[(1-\nu)E_{\alpha\beta}+\nu E_{\gamma\gamma}\delta_{\alpha\beta}]\\ \text{and}\quad M_{\alpha\beta} &= D[(1-\nu)K_{\alpha\beta}+\nu K_{\gamma\gamma}\delta_{\alpha\beta}],\end{aligned}\right\} \tag{2.7}$$

with t as the shell thickness, E as Young's modulus, v as Poisson's ratio and $D = Et^3/[12(1-v)^2]$ as the bending stiffness. The resultant membrane stresses are $(N_{\omega\omega}, N_{\theta\theta}, N_{\omega\theta})$ and the bending moments are $(M_{\omega\omega}, M_{\theta\theta}, M_{\omega\theta})$. With S denoting the reference spherical surface specified by $r = R$ and the Euler angles (ω, θ), the elastic energy in the shell is

$$\mathrm{SE}(u_\omega, u_\theta, w) = \frac{1}{2}\int_S \{M_{\alpha\beta}K_{\alpha\beta} + N_{\alpha\beta}E_{\alpha\beta}\}\mathrm{d}S. \tag{2.8}$$

For the perfect shell, the potential energy (PE) of the uniform inward pressure p on the shell is the negative of the work done by the pressure. For *dead pressure* (force per unit original area of the middle surface acting in the original radial direction),

$$\mathrm{PE} = p\int_S w\,\mathrm{d}S \quad \text{(dead pressure)}. \tag{2.9}$$

For *live pressure* (force per area of the deformed middle surface acting normal to the deformed middle surface), the PE is the pressure multiplied by the change of volume ΔV within the middle surface. The results in [15,16,18] can be used to obtain the following exact expression for ΔV in terms of the middle surface displacements and their gradients, here in the surface tensor notation of [18]:

$$\Delta V = \int_S \left\{ w + \frac{1}{3}[(\varphi^\alpha + Q^\alpha)u_\alpha + R(\varphi_r^2 + |e_\beta^\alpha|) + w(e_\alpha^\alpha + |e_\beta^\alpha| + \varphi_r^2)] \right\} \mathrm{d}S, \tag{2.10}$$

with $|e_\beta^\alpha|$ as the determinant of e_β^α, $Q^\alpha = \varphi^\alpha e_\beta^\beta - \varphi^\beta e_\beta^\alpha + \varepsilon^{\beta\alpha}\varphi_\beta\varphi_r$ and $\varepsilon^{\alpha\beta}$ as the surface alternating tensor. We omit listing this expression in terms of physical components as it is rather lengthy. However, in physical components for axisymmetric deformations, (2.10) becomes

$$\Delta V = \int_S \left\{ w + \frac{1}{3}[(1 + e_{\omega\omega})\varphi_\theta u_\theta + w(e_{\omega\omega} + e_{\theta\theta}) + (R + w)e_{\omega\omega}e_{\theta\theta}] \right\} \mathrm{d}S. \tag{2.11}$$

These exact results, (2.10) and (2.11), are applicable to a full spherical shell or any segment of the shell which is constrained such that u_ω and u_θ vanish on the boundary. The integrand in each of the expressions for ΔV is a cubic function of the displacements and their gradients. It is worth recording that a general expression for ΔV in [17], an alternative to that in (2.10), appears to include errors or misprints.

Now introduce the effect of an axisymmetric initial imperfection w_I on the PE of the pressure loading using the process described for the strains, where w becomes additional to w_I. Because it is linear in w, the PE for dead pressure remains as (2.9). For live pressure, the resulting expressions derived from (2.10) or (2.11) involving w_I are lengthy and will not be listed. The energy functional of the loaded shell system is

$$\Psi = \mathrm{SE}(u_\omega, u_\theta, w) + pf(u_\omega, u_\theta, w), \tag{2.12}$$

where $\mathrm{PE} = pf$, with f given by (2.9) for dead pressure or derived from (2.10) or (2.11) for live pressure. The presence of w_I in (2.12) is not explicitly noted.

(b) Donnell–Mushtari–Vlasov theory

DMV theory introduces two approximations to the moderate rotation theory: (i) the square of the rotation about the normal, φ_r^2, is neglected in the in-plane strains (2.6) and (ii) the deformations are assumed to have a short wavelength relative to R, referred to as shallow deformations, such that the displacements u_ω and u_θ in the rotations φ_ω and φ_θ in (2.3) are neglected. Thus, in DMV

theory for spherical shells with small axisymmetric initial imperfections, the strain–displacement relations are

$$\left.\begin{aligned} E_{\omega\omega} &= e_{\omega\omega} + \frac{1}{2}\left(\frac{1}{R\cos\theta}\frac{\partial w}{\partial \omega}\right)^2, \\ E_{\theta\theta} &= e_{\theta\theta} + \frac{1}{2}\left(\frac{1}{R}\frac{\partial w}{\partial \theta}\right)^2 - \frac{1}{R}\frac{\mathrm{d}w_{\mathrm{I}}}{\mathrm{d}\theta}\varphi_\theta \\ \text{and}\quad E_{\omega\theta} &= e_{\omega\theta} + \frac{1}{2}\left(\frac{1}{R\cos\theta}\frac{\partial w}{\partial \omega}\right)\left(\frac{1}{R}\frac{\partial w}{\partial \theta}\right) - \frac{1}{2R}\frac{\mathrm{d}w_{\mathrm{I}}}{\mathrm{d}\theta}\varphi_\omega \end{aligned}\right\} \tag{2.13}$$

and

$$\left.\begin{aligned} K_{\omega\omega} &= -\frac{1}{R^2\cos\theta}\left(\frac{\partial^2 w}{\partial \omega^2} - \sin\theta\,\frac{\partial w}{\partial \theta}\right), \\ K_{\theta\theta} &= -\frac{1}{R^2}\frac{\partial^2 w}{\partial \theta^2} \\ \text{and}\quad K_{\omega\theta} &= -\frac{1}{R^2}\left(\frac{\partial^2 w}{\partial \omega\,\partial \theta} + \tan\theta\frac{\partial w}{\partial \omega}\right), \end{aligned}\right\} \tag{2.14}$$

where the linearized stretching strains in (2.13) are still given by (2.2).

Generally only dead pressure is represented when DMV theory is used with PE given by (2.9). The stress–strain relations are given by (2.7) and the elastic strain energy by (2.8). Thus, for DMV theory, the energy functional for the spherical shell subject to uniform pressure is given by (2.12) with $f = \int_S w\,\mathrm{d}S$.

(c) Exact first-order theory for axisymmetric deformations

The stretching and bending strain measures of moderate rotation theory and DMV theory are approximate and their accuracy deteriorates as the shell displacements and rotations become sufficiently large. The following expressions for the Lagrangian stretching strains, ($E_{\omega\omega}$, $E_{\theta\theta}$), and changes in curvature, ($K_{\omega\omega}$, $K_{\theta\theta}$), of the spherical shell middle surface are exact and can be obtained from [15,16,18]. A first-order shell theory based on these exact measures will be used to benchmark the other two theories using approximate strain measures by illustrating the range over which the measures remain accurate. The exact measures are limited to axisymmetric deformations ($u_\omega = 0$, $u_\theta(\theta)$, $w(\theta)$). The linearized stretching strains, ($e_{\omega\omega}$, $e_{\theta\theta}$), and rotation, φ_θ, are defined in (2.2) and (2.3), respectively. The Lagrangian stretching strains are

$$\left.\begin{aligned} E_{\omega\omega} &= e_{\omega\omega} + \tfrac{1}{2}e_{\omega\omega}^2 \\ \text{and}\quad E_{\theta\theta} &= e_{\theta\theta} + \tfrac{1}{2}{e_{\theta\theta}}^2 + \tfrac{1}{2}\varphi_\theta^2, \end{aligned}\right\} \tag{2.15}$$

while the changes in curvature are

$$K_{\omega\omega} = \frac{1}{R}\{(1 + e_{\omega\omega} + e_{\theta\theta} + e_{\omega\omega}e_{\theta\theta})(1 - \tan\theta\,\varphi_\theta + e_{\omega\omega}) + \tan\theta\,\varphi_\theta(1 + e_{\omega\omega})(e_{\theta\theta} - e_{\omega\omega}) - 1\} \tag{2.16}$$

and

$$K_{\theta\theta} = \frac{1}{R}\left\{(1 + e_{\omega\omega} + e_{\theta\theta} + e_{\omega\omega}e_{\theta\theta})\left(1 + \frac{\mathrm{d}\varphi_\theta}{\mathrm{d}\theta} + e_{\theta\theta}\right) - \varphi_\theta(1 + e_{\omega\omega})\left(\frac{\mathrm{d}e_{\theta\theta}}{\mathrm{d}\theta} - \varphi_\theta\right) - 1\right\}. \tag{2.17}$$

Consistent with a first-order theory for a material with a linear stress–strain response, the membrane and bending stresses are still given by (2.7). In all the problems investigated in this paper, the stretching strains, $E_{\omega\omega}$ and $E_{\theta\theta}$, remain small. Thus, the distinction between the Lagrangian strains and other measures is insignificant and the linear constitutive relation (2.7) is meaningful. The strain energy, PE of the live pressure loading and the energy functional Ψ of the system have the same forms as those given earlier for the moderate rotation theory in (2.12).

3. Bifurcation pressure and modes for the perfect shell based on Donnell–Mushtari–Vlasov theory

Koiter [1] cites the PhD thesis of van der Neut [19] as the first rigorous demonstration that the eigenvalue problem for the buckling of a perfect spherical shell subject to uniform pressure has simultaneous axisymmetric and non-axisymmetric eigenmodes with bifurcation from the uniformly compressed state at the critical pressure

$$p_C = \frac{2E}{\sqrt{3(1-\nu^2)}}\left(\frac{t}{R}\right)^2. \tag{3.1}$$

Koiter [1] provides his own derivation of van der Neut's results using moderate rotation theory but in so doing invokes a series of approximations that follow from the fact that the eigenmodes are shallow, i.e. have short wavelengths relative to R. His derivation is tantamount to invoking DMV theory. It is insightful and useful for present purposes to provide a derivation of the classical results for buckling of a perfect spherical shell using DMV theory from the start. This section provides that derivation. We will demonstrate later in this paper that DMV theory with dead pressure loading is accurate for nearly all aspects of the buckling behaviour of interest in this paper.

The uniform membrane solution for the perfect spherical shell subject to uniform pressure p according to either moderate rotation theory or DMV theory is

$$u_\omega = u_\theta = 0,\ w^0 = -\frac{(1-\nu)pR^2}{2Et} \quad \text{with } N^0_{\omega\omega} = N^0_{\theta\theta} = -\sigma t \quad \text{and} \quad \sigma = \frac{1}{2}p\frac{R}{t}, \tag{3.2}$$

where σ is the equi-biaxial compressive stress in the shell in the uniform state. Bifurcation from this uniform state in the form $(u_\omega, u_\theta, w) = (\Delta u_\omega, \Delta u_\theta, w^0 + \Delta w)$ is sought where the nonlinear equations are linearized about the uniform state with respect to the Δ-quantities. The well-known formulation using the Airy stress function ΔF to satisfy in-plane equilibrium is employed along with the additional compatibility condition. The perturbation process leads to a pair of coupled partial differential equations from DMV theory governing the buckling eigenvalue problem

$$D\nabla^4\Delta w + \frac{1}{R}\nabla^2\Delta F + \sigma t\nabla^2\Delta w = 0 \quad \text{and} \quad \frac{1}{Et}\nabla^4\Delta F - \frac{1}{R}\nabla^2\Delta w = 0, \tag{3.3}$$

where ∇^2 is the Laplacian operator on the spherical reference surface and $\nabla^4 = \nabla^2(\nabla^2)$. Eliminating ΔF from the pair of equations in (3.3) gives

$$\nabla^2\left\{D\nabla^4\Delta w + \frac{Et}{R^2}\Delta w + \sigma t\nabla^2\Delta w\right\} = 0. \tag{3.4}$$

The spherical harmonic $S_{nm}(\omega,\theta) = \left(\begin{smallmatrix}\sin m\omega\\ \cos m\omega\end{smallmatrix}\right) P^m_n(\sin\theta)$, with P^m_n as the associated Legendre function of degree n and order m, satisfies $\nabla^2 S_{nm} = -n(n+1)R^{-2}S_{nm}$. With n and m $(0 \le m \le n)$ restricted to be integers to ensure circumferential continuity and smooth behaviour at the poles, it follows from (3.4) that eigenmodes of the form $w \propto S_{nm}$ are associated with the eigenvalue

$$\frac{\sigma tR^2}{D} = n(n+1) + q_0^4\frac{1}{n(n+1)} \quad \text{with } q_0^4 = 12(1-\nu^2)\left(\frac{R}{t}\right)^2. \tag{3.5}$$

Anticipating that for thin shells n will be reasonably large, $x = n(n+1)$ can be regarded as a continuous variable, ignoring the fact that n must be an integer, to minimize σ with respect to x. This provides a lower bound estimate of the lowest eigenvalue, i.e. the buckling stress and

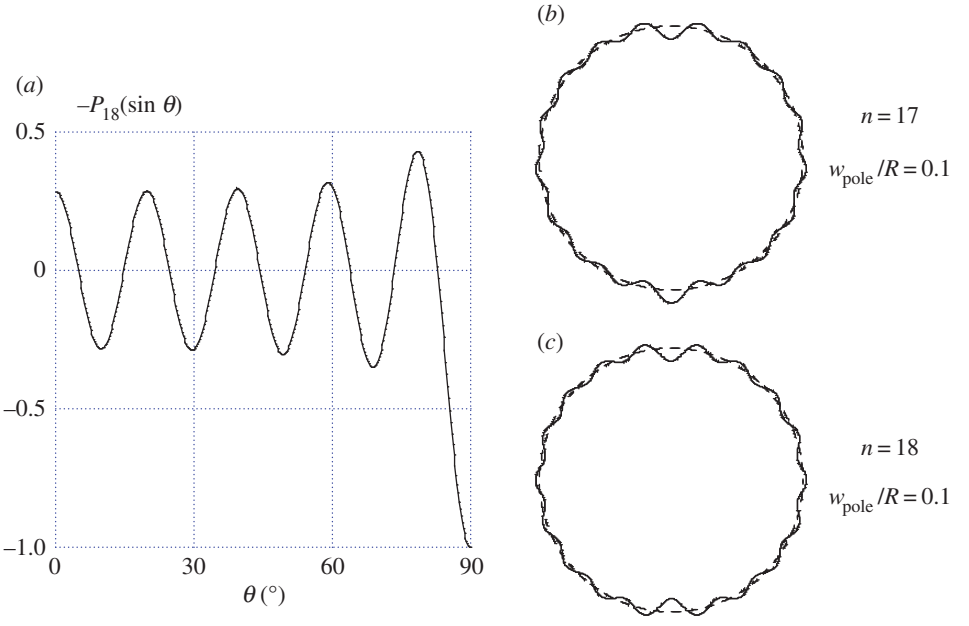

Figure 1. In (*a*,*c*), the symmetric axisymmetric bifurcation mode for the perfect shell with $R/t = 103.5$ and $\nu = 0.3$. In (*b*), the antisymmetric axisymmetric bifurcation mode for $R/t = 92.6$ and $\nu = 0.3$. (Online version in colour.)

pressure for the perfect shell,

$$\left.\begin{aligned} \sigma_C &= \frac{E}{\sqrt{3(1-\nu^2)}}\frac{t}{R}, \\ p_C &= \frac{2E}{\sqrt{3(1-\nu^2)}}\left(\frac{t}{R}\right)^2 \\ \text{and} \qquad n(n+1) &= \sqrt{12(1-\nu^2)}\frac{R}{t}. \end{aligned}\right\} \tag{3.6}$$

This reproduces the result in [1]. For R/t values for which n is an integer, (3.6) is the lowest eigenvalue. However, as Koiter [1] notes, for other values of R/t the difference between the lower bound in (3.6) and the slightly larger eigenvalue for integer n is of relative order t/R. This difference is very small for thin shells such that σ_C and p_C in (3.6) are universally referred to as the critical buckling stress and pressure of the perfect shell. Moreover, numerical calculations with the moderate rotation theory with either live or dead pressure along the lines of those reported later reveal that, even for a shell with R/t as small as 50, the difference between the classical formulae for σ_C and p_C in (3.6) and the lowest eigenvalue computed based on integer n is never more than 1%.

There are $2n+1$ modes associated with the lowest eigenvalue: the axisymmetric mode, $m=0$ and $w = P_n^0(\sin\theta) \equiv P_n(\sin\theta)$, and $2n$ non-axisymmetric modes, $w = \cos m\omega\, P_n^m(\sin\theta)$ and $w = \sin m\omega\, P_n^m(\sin\theta)$ with $1 \le m \le n$. The shape of the axisymmetric mode is shown in figure 1 for shells with $\upsilon = 0.3$, in one case with $R/t = 103.5$ corresponding to a mode ($n = 18$) that is symmetric about the equator and in the other case with $R/t = 92.6$ having an antisymmetric mode ($n = 17$). Throughout this paper, the inward deflection at the upper pole is defined as $w_{pole} = -w(\pi/2)$. In figure 1*b*,*c*, the shape is plotted with $w_{pole}/R = 0.1$ for visualization purposes. As will be seen, this far exceeds the amplitude for which the bifurcation mode has any relevance.

The coupling of the multiple modes in the nonlinear post-buckling range is one of the reasons for the extremely strong imperfection sensitivity of the buckling of the spherical shell under external pressure [1,3]. It will be useful at this stage to make contact with Hutchinson's

[20] analysis based on the behaviour of interacting modes in the vicinity of the shell equator. Let $w = \cos m\omega\, \bar{w}(\theta)$ be any eigenmode with $\bar{w}(\theta) \propto P_n^m(\sin\theta)$, with $\bar{w}$ satisfying the equation for Legendre's associated functions,

$$\frac{1}{\cos\theta}\frac{\mathrm{d}}{\mathrm{d}\theta}\left(\cos\theta\frac{\mathrm{d}\bar{w}}{\mathrm{d}\theta}\right) + \left(n(n+1) - \frac{m^2}{\cos^2\theta}\right)\bar{w} = 0. \tag{3.7}$$

Near the equator where $\theta \approx 0$, (3.7) is approximated by

$$\frac{\mathrm{d}^2\bar{w}}{\mathrm{d}^2\theta} + (n(n+1) - m^2)\bar{w} = 0. \tag{3.8}$$

Thus, in the vicinity of the equator, symmetric modes have $\bar{w}(\theta) = \cos\left(\sqrt{q_0^2 - m^2}\theta\right)$ apart from a different multiplicative factor where, by (3.5) and (3.6), $n(n+1) = q_0^2$. With ℓ_ω and ℓ_θ denoting the wavelengths of the mode in the circumferential and meridional directions, the simultaneous symmetric modes in the vicinity of the equator have the form

$$w = \cos\left(\frac{2\pi R\omega}{\ell_\omega}\right)\cos\left(\frac{2\pi R\theta}{\ell_\theta}\right) \quad \text{with} \left(\frac{2\pi R}{\ell_\theta}\right)^2 + \left(\frac{2\pi R}{\ell_\omega}\right)^2 = q_0^2. \tag{3.9}$$

These are the modes considered in the analysis of mode interaction and imperfection sensitivity in shallow sections of a sphere [20]. The buckle wavelengths are of the order of $\ell \approx \sqrt{Rt}$ and small compared with R for thin shells. This representation of the modes will be used in the sequel.

4. Axisymmetric post-buckling behaviour of the perfect shell

Selected results for the axisymmetric post-buckling behaviour of the perfect shell will be presented emphasizing behaviour at both small and large deflections. From a structural standpoint, it will be seen that the important action occurs at small deflections that are usually not more than several times the shell thickness. The numerical results in this paper make use of highly effective algorithms (see appendices) for solving nonlinear ODEs which were not available in the 1960s when nearly all the prior studies of spherical shell buckling were carried out. Koiter's [1] study of the imperfection sensitivity of spherical shell buckling employed analytical methods based on perturbation expansions about the bifurcation point of the perfect shell, although he attempted to extend the range of validity of these expansions by analytical means.

We begin by presenting an example of axisymmetric large deflection behaviour based on the formulation in §2c that employs exact middle surface strain measures. The numerical method for this formulation is described in the appendices. The shells in figure 2 have $R/t = 25$ and 50 with $v = 0.3$. Symmetry with respect to the equator has been imposed. Following bifurcation, the pressure falls monotonically to the point where the opposite poles make contact. Under prescribed pressure, the post-buckling response would be unstable over the entire range of deformation plotted. Even under prescribed volume change ΔV, the response at bifurcation is unstable until the pressure drops to $p/p_C \cong 0.2$ ($w_{\text{pole}}/R \cong 0.3$) for $R/t = 25$ or $p/p_C \cong 0.15$ ($w_{\text{pole}}/R \cong 0.2$) for $R/t = 50$. The post-buckling shape seen in the insert in figure 2*a* does not resemble the classical axisymmetric mode described in §3 for reasons which will be discussed shortly. Instead, the advanced buckling shape in the vicinity of the pole is approximately an inverted cap with radius of curvature $-R$. For sufficiently small pole deflections, the buckle is shallow and the rotation of the middle surface is small. However, as the pole deflection increases, the magnitude of the maximum rotation becomes larger than 90° in the limit when $w_{\text{pole}}/R = 1$, clearly exceeding the range in which moderate rotation theory is expected to hold.

An important point brought out in figure 3 is that much of the essential buckling behaviour of thin shells plays out in the range of deflections of the order of several shell thicknesses. The solid line curves in figure 3 have been computed using the moderate rotation theory of §2b together with live pressure using the exact expression (2.11) for the change in volume. For axisymmetric deformations, the small strain–moderate rotation equations reduce to the system of six nonlinear

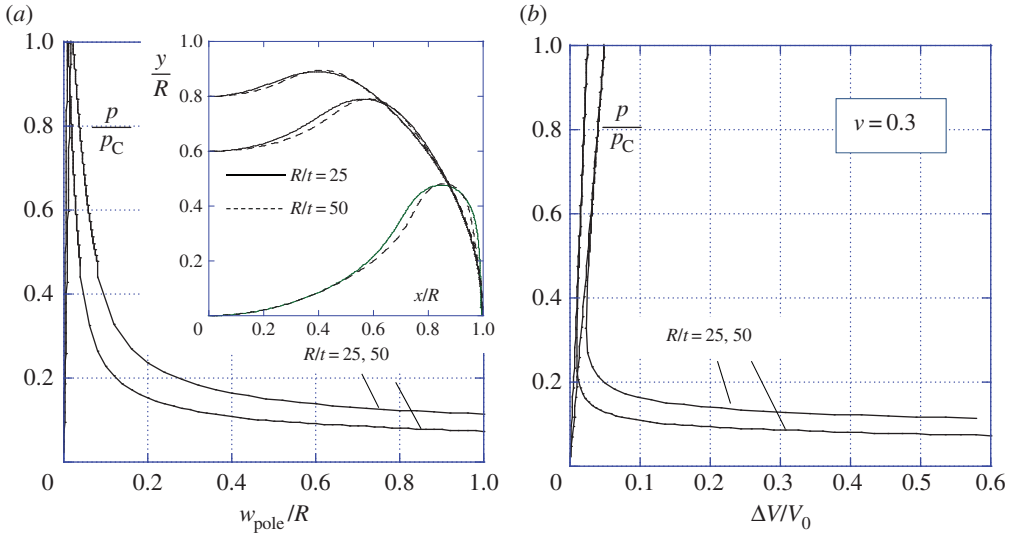

Figure 2. Large axisymmetric deflections of two perfect shells based on the exact formulation. (*a*) Pressure versus pole deflection normalized by the sphere radius. (*b*) Pressure versus change in volume normalize by the negative of the volume within the middle surface of the undeformed sphere, $V_0 = -4\pi R^3/3$. The deformed middle surface is plotted in the insert in (*a*) at three levels of deformation, including that at which the opposing poles first make contact. (Online version in colour.)

first-order ODEs given in the appendices. The dashed line curves in figure 3 have been computed using the exact formulation for the case $R/t = 50$. For this case, divergence between the moderate rotation theory and exact theory for the linearized rotation φ_θ is first evident at 0.25 radians ($\cong 15°$) but is still relatively small at twice that level. In fact, the moderate rotation prediction for the relation of the pressure to the pole deflection for $R/t = 50$ remains accurate for pole deflections as large as $w_{\text{pole}}/t = 10$ or $w_{\text{pole}}/R = 0.2$. The same is true for the relation of pressure to change in volume. Equally important is the observation that, in the range of behaviour plotted, the relation of p/p_C to w_{pole}/t is essentially independent of R/t and becomes increasingly so for even larger R/t. As evident from figure 3*c*, the relation of p/p_C to $\Delta V/V_C$ is not independent of R/t due to the fact that the dimple-like buckle at the pole diminishes in size relative to the sphere as R/t increases. A complete characterization of this behaviour will be given in a subsequent publication.

For spherical shell buckling, it appears that the moderate rotation theory retains a reasonably high level of accuracy for the main quantities of interest for deflections considerably beyond those based on the previously quoted rule of thumb that the rotations should not exceed 15–20°. All of the subsequent results presented in this paper lie within the range $w_{\text{pole}}/t \leq 10$ and they have been computed with the moderate rotation theory of §2b. Selected results have been recomputed using the less accurate DMV theory. Apart from one case involving non-axisymmetric bifurcation, we have not observed any appreciable difference between the predictions of the two theories. Moreover, except for the very large deflection results in figure 2, there is almost no difference between imposing live or dead pressure for the moderate rotation theory for any of the other results presented in this paper. Finally, and importantly, the possibility of non-axisymmetric bifurcation from the axisymmetric state will be analysed in §7 and reported for all the axisymmetric solutions based on the moderate rotation theory. In particular, non-axisymmetric bifurcation from the axisymmetric post-buckling solutions in figure 3 does not occur. Once initiated these axisymmetric solutions are resistant to non-axisymmetric bifurcation and remain axisymmetric.

We end this section on buckling of the perfect spherical shell by displaying the extraordinarily rapid transition from the classical bifurcation mode seen in figure 1 to the localized dimple-like mode seen in the insert in figure 2*a*. For this purpose, a perfect shell with $R/t = 103.5$ and $v = 0.3$ is considered, corresponding exactly to $n = 18$ by (3.6) and to the axisymmetric bifurcation mode

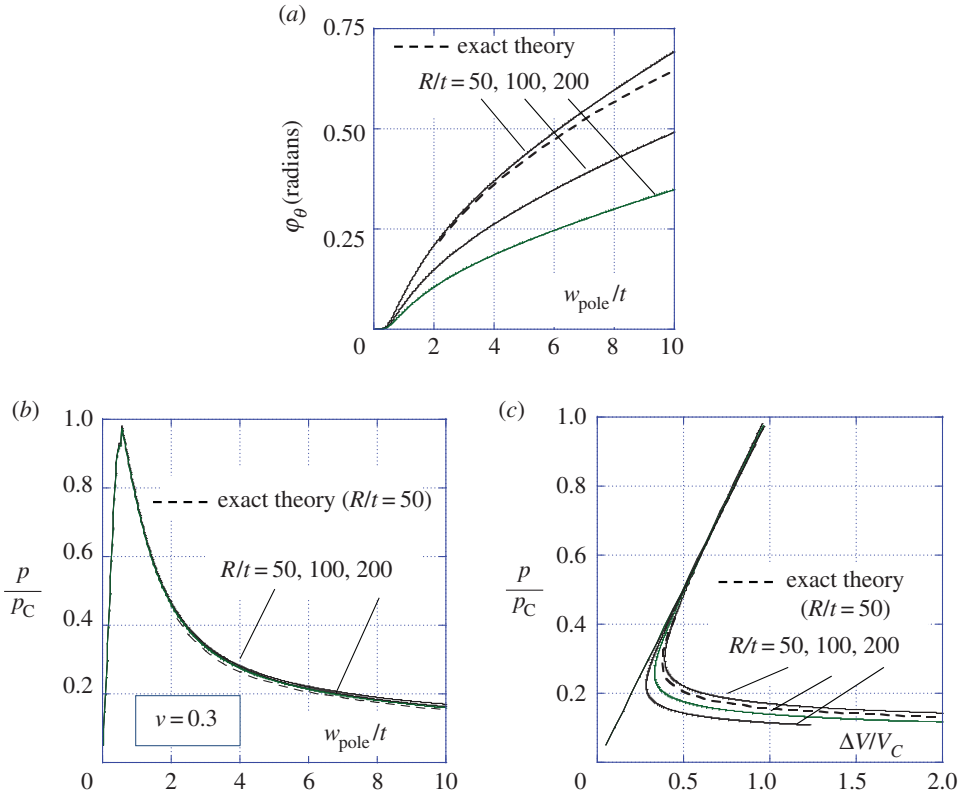

Figure 3. Axisymmetric post-buckling behaviour of the perfect shell in the range of relatively small deflections for shells with several R/t, assuming symmetry with respect to the equator. Solid lines denote results based on moderate rotation theory and dashed lines are based on the exact formulation for $R/t = 50$. In (*c*), $\Delta V_C = 4\pi R^2 w_C$ is the change of volume of the perfect shell at bifurcation where the associated normal displacement is $w_C = -(1-\nu)t/\sqrt{3(1-\nu^2)}$. An extremely small initial imperfection is used to trigger bifurcation from the spherical shape. This imperfection is then reduced to zero on the post-bifurcation branch. (Online version in colour.)

shown in figure 1*a*,*c*. The dramatic evolution of the post-bifurcation buckling mode is shown in figure 4. Almost immediately following bifurcation, the classical mode gives way to a dimple-like mode localized at the pole. The deflection over most of the shell away from the pole is simply the uniformly compressed state. As discussed in connection with figure 2, this dimple becomes an inverted cap near the pole with radius of curvature approaching $-R$. Evkin *et al*. [21] have presented an asymptotic analysis of the dimple mode using shallow shell theory applicable to thin spherical shells in which the dimple is confined to the vicinity of the pole. Based on their asymptotic analysis, the authors derive a formula for the dependence of p/p_C on w_{pole}/t. Their formula is independent of R/t and reproduces the results in figure 3*b* with an error as large as 25% for moderate values of w_{pole}/t but becoming increasingly accurate as w_{pole}/t becomes larger. Further details of the asymptotic results in [21] will be discussed in a subsequent publication.

The immediate localization of the post-buckling mode to the pole of the sphere was not well understood to researchers in the 1960s, although there is already recognition by von Karman & Tsien [2] that experimentally observed buckling modes were more dimple-like than shaped like the classical mode. The localization explains why the initial post-bifurcation expansions of Thompson [4] and Koiter [1] based on the axisymmetric classical bifurcation mode have such an exceptionally small domain of validity. The initial post-bifurcation approach tacitly assumes that the classical bifurcation mode provides the first-order, and dominant, approximation to the post-buckling mode. As soon as mode localization occurs, this ceases to be a good assumption. While

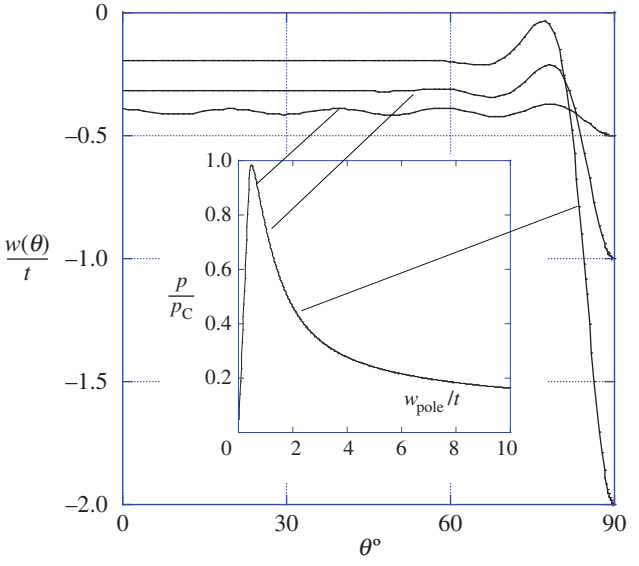

Figure 4. Evolution of the buckling mode in the initial post-bifurcation range for a perfect spherical shell with $R/t = 103.5$ and $\nu = 0.3$ with indicators pointing to the associated location on the pressure–deflection curve. The classical bifurcation mode with $w_{\text{bif}} \propto P_{18}(\sin\theta)$ is evident only for an extremely small range beyond bifurcation whereupon the mode becomes fully localized at the pole to an inward dimple-like shape. (Online version in colour.)

evidently not aware of the localization phenomenon, Koiter was aware that the range of validity of the expansions was severely limited for sphere buckling. A substantial portion of his study [1] was devoted to an attempt to extend the validity of the expansions.

5. The effect of axisymmetric imperfections in the shape of the classical mode

Because imperfections in the shape of the classical bifurcation mode are known to cause the largest load reductions in imperfection-sensitive structures [3], at least for sufficiently small imperfection amplitudes, we begin by considering axisymmetric imperfections of the form $w_{\text{I}}(\theta) = -\delta\, P_n(\sin\theta)$, where δ is the imperfection amplitude and n is related to R/t by (3.6). In the next section, it will be seen that dimple-shaped imperfections are more critical for all but small imperfection amplitudes.

The example in figure 5 shows the effect of different imperfection amplitudes on the post-buckling response of a shell with $R/t = 103.5$ and $\nu = 0.3$ corresponding to $n = 18$ and $w_{\text{I}}(\theta) = -\delta\, P_{18}(\sin\theta)$. The imperfection shape plotted in figure 1*a* has its largest magnitude at the poles with $w_{\text{I}}(\pm\pi/2) = -\delta$. Shells having imperfections with amplitudes less than $\delta/t = 0.5$ display a pressure maximum, $p_{\max}$, in the early stage of deformation at $w_{\text{pole}}/t \approx 1$ followed by diminishing pressure with increasing buckling amplitude. Under prescribed pressure, the shell would become unstable and undergo snap buckling at $p_{\max}$. The shells become unstable just beyond attainment of $p_{\max}$ even under prescribed volume change for sufficiently small imperfections, i.e. $\delta/t < \approx 0.25$. An unexpected finding is the fact that shells with imperfections equal to or larger than approximately $\delta/t = 0.5$ have no pressure maximum in the early stage of deformation. For these shells, the pressure increases gradually until a peak is finally attained at much larger deflections, e.g. $w_{\text{pole}}/t \cong 10$, as illustrated by the example in figure 5.

The normalized maximum pressure, $p_{\max}/p_{\text{C}}$, as a function of the imperfection amplitude, δ/t, for four values of R/t is plotted in figure 6. The imperfection for each R/t is again taken to be $w_{\text{I}} = -\delta\, P_n(\sin\theta)$, where the integer n is given exactly in terms of R/t by (3.6). Each case corresponds to an even value of n and symmetry about the equator is invoked in the computations carried out using the moderate rotation theory. As noted in connection with the example in

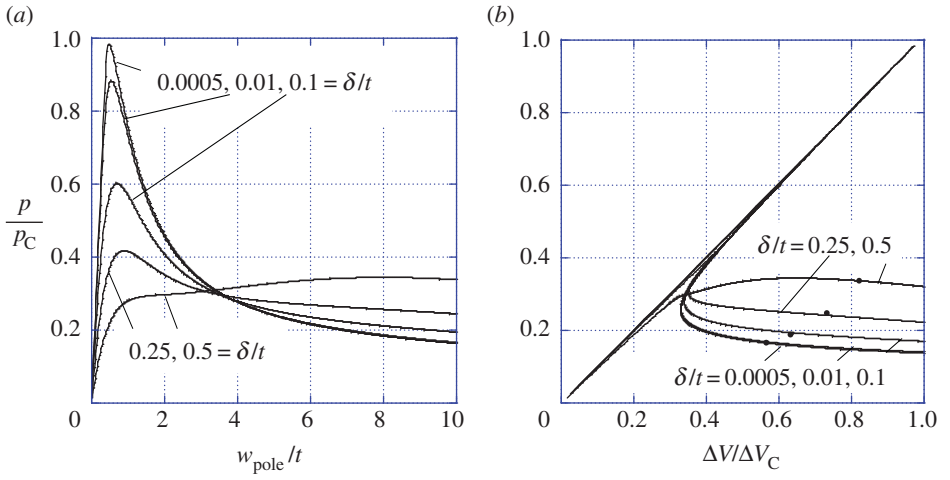

Figure 5. Plots of the pressure versus (*a*) the displacement at the pole and (*b*) the change in volume of the shell, for shells with $R/t = 103.5$ and $\nu = 0.3$. Results are shown for five levels of imperfection, $w_I = -\delta\, P_{18}(\sin\theta)$, where the imperfection is in the shape of the buckling deflection of the perfect shell (cf. figure 1*a*,*c*). The results in (*b*) have been computed to values of $w_{\text{pole}}/t > 10$; the solid dot on each curve indicates where $w_{\text{pole}}/t = 10$. (Online version in colour.)

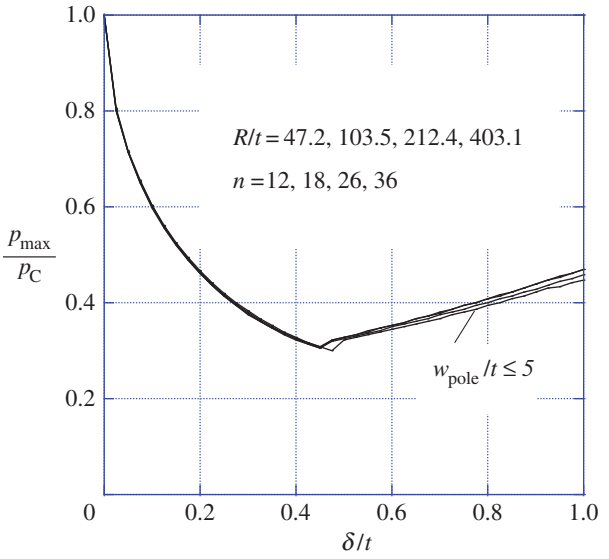

Figure 6. Imperfection–sensitivity for shells having imperfections in the shape of the classical axisymmetric buckling mode, $w_I = -\delta\, P_n(\sin\theta)$. Results for four values of R/t have been plotted and are almost indistinguishable from one another. For imperfection amplitudes satisfying $\delta/t < 0.45$, $p_{\max}$ is the pressure maximum attained at pole deflections never larger than $w_{\text{pole}}/t \cong 1.5$. For $\delta/t > 0.45$, the value of $p_{\max}$ plotted is either the pressure maximum, if one occurs, or the value of p attained at $w_{\text{pole}}/t = 5$ if a maximum has not yet been obtained. (Online version in colour.)

figure 5, $p_{\max}$ is associated with a clearly defined peak pressure at relative small buckling deflection, e.g. $w_{\text{pole}}/t < 1.5$, for smaller amplitude imperfections satisfying $\delta/t < 0.45$. For larger δ/t in figure 6, no peak pressure is attained in the range of small buckling deflections. Thus, for $\delta/t > 0.45$, the range of pole deflections has been limited to $w_{\text{pole}}/t \leq 5$ and $p_{\max}$ is either the peak pressure, if one occurs in this range, or the value of p at $w_{\text{pole}}/t = 5$. Two notable features

are evident in figure 6. First, for $\delta/t > 0.45$, increasing the imperfection amplitude *increases* the buckling pressure. Second, the imperfection-sensitivity curves are nearly independent of R/t, increasingly so as R/t increases beyond 100. The issue of non-axisymmetric buckling from the axisymmetric state will be addressed in §7. Except for the largest imperfections in figure 6 in the range $\delta/t > 0.9$, non-axisymmetric bifurcation does not occur at pressures lower than $p_{\max}$ plotted. In fact, over most of the range for $\delta/t < 0.9$, non-axisymmetric bifurcation does not occur even at deflections well beyond the maximum pressure. In the range $\delta/t > 0.9$, non-axisymmetric bifurcation does occur just prior to attaining $p_{\max}$ in figure 6, implying that buckling in a non-axisymmetric mode would be initiated. For example, for $\delta/t = 1$, $p_{\text{bif}}/p_{\text{C}} = 0.39$ ($m = 8$) for $R/t = 47.2$ and $p_{\text{bif}}/p_{\text{C}} = 0.41$ ($m = 8$) for $R/t = 103.5$.

Two aspects of axisymmetric spherical shell buckling described thus far have not been revealed in earlier studies: (i) the nature of the localization transition of the buckling mode at the pole in the post-buckling response almost immediately after the onset of buckling and (ii) the unexpected increase in load-carrying capacity with increasing imperfection amplitude seen in figures 5 and 6 for the larger imperfections. Neither aspect could be expected to be uncovered from Koiter's [1] analytical approach for reasons already discussed. Koga & Hoff [22] were among the last investigators in the 1960s to provide numerical results for the axisymmetric buckling of spherical shells with axisymmetric dimple-like imperfections, but their method was not accurate and their results overestimate the reduction in buckling load due to the imperfection. Moreover, the largest imperfection amplitude these authors considered was $\delta/t = 0.5$.

Numerical analysis is a powerful tool for accurately capturing the nonlinear phenomena revealed here associated with spherical shell bucking, particularly because much interesting behaviour is axisymmetric and therefore governed by nonlinear ODEs. It should be mentioned that numerical analysis codes did exist beginning in the late 1960s which were capable of uncovering the behaviour brought out in figures 5 and 6. Specifically, Bushnell [23] developed accurate methods for solving nonlinear axisymmetric problems for shells of revolution which later evolved into the BOSOR code [24]. Non-axisymmetric bifurcation from the axisymmetric state could also be addressed by BOSOR. While this and other numerical codes had the capabilities needed to advance the understanding of spherical shell buckling five decades ago, such studies were not carried out. Upon completion of this paper, it came to our attention that Bushnell, in his PhD thesis [25], carried out an extensive numerical analysis of the axisymmetric buckling of clamped shallow spherical caps that did reveal the localization transition discussed above for caps with sufficient height. Other than appearing in Bushnell's thesis, this work has not been published.

6. Imperfection sensitivity for dimple imperfections

Motivated by the tendency of the buckling mode to localize at the pole, attention is again focused on axisymmetric behaviour of the shell but now for dimple imperfections located at the poles specified by

$$w_I(\theta) = -\delta\, \mathrm{e}^{-(\beta/\beta_{\text{I}})^2} \quad \text{with } \beta = \theta - \frac{\pi}{2} \text{ (at the upper pole).} \tag{6.1}$$

Here, β_{I} sets the width of the imperfection. In all cases, the imperfection becomes exponentially small for $\beta \gg \beta_{\text{I}}$ and is effectively zero at the equator. Attention is limited to deflections which are symmetric about the equator. The localized nature of the buckling decouples behaviour above the equator from that below, and there is essentially no difference in the imperfection sensitivity for the symmetric case having identical imperfections at each pole and that for an asymmetric case, for example, with the imperfection at only one pole.

Critical buckling wavelengths are proportional to $\sqrt{Rt}$, such that the scaling

$$\beta_{\text{I}} = \frac{B}{\left(\sqrt{1-\nu^2}R/t\right)^{1/2}} \tag{6.2}$$

ensures that the imperfection–sensitivity will be essentially independent of R/t, as will be seen.

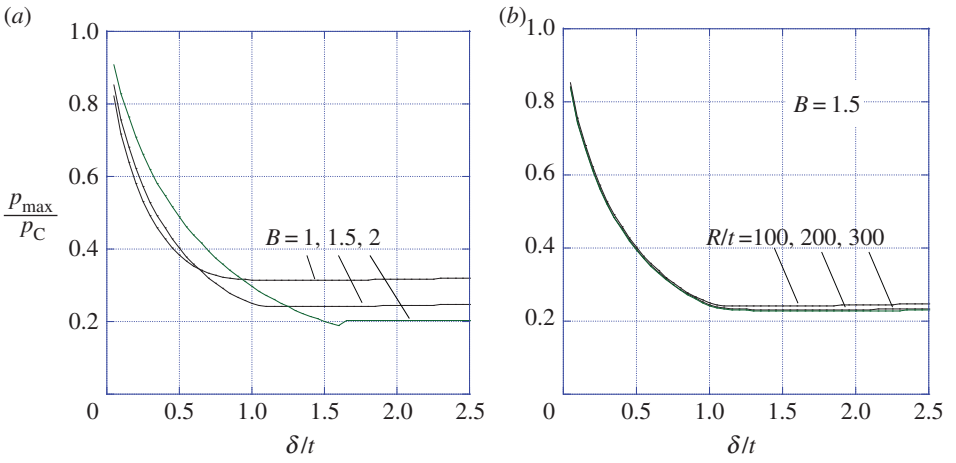

Figure 7. Imperfection–sensitivity based on axisymmetric buckling for dimple imperfections (6.1). (*a*) Shells with $R/t = 100$, $\nu = 0.3$ and three imperfection widths set by B in (6.2). (*b*) Shells with different R/t, with $B = 1.5$ and dimple width scaling according to (6.2). For $B = 2$ and $\delta/t > 1.6$ in (*a*), a maximum pressure at modest deflections does not occur and p_{max} is defined as the pressure at $w_{pole}/t = 5$. In all other cases, including those in (*b*), p_{max} is associated with a pressure maximum attained for buckling deflections satisfying $w_{pole}/t < 5$. (Online version in colour.)

Plots of imperfection–sensitivity for three widths of the dimple imperfection are given in figure 7*a* for $R/t = 100$. For relatively small amplitudes, e.g. $\delta/t < 0.5$, imperfections with width specified by $B \cong 1$ give the largest reductions in buckling pressure, while for larger amplitudes the largest reductions are caused by somewhat wider imperfections with $B > 1$. In almost all the cases in figure 7, p_{max} is associated with a well-defined peak pressure, such as those cases shown in figure 5, occurring at relatively small pole deflections. The only exceptions are the shells with $B = 2$ and $\delta/t > 1.6$ where no peak occurs at modest deflections. In these cases, p_{max} is defined as either the maximum, if one occurs, or the pressure at $w_{pole}/t = 5$, if no maximum has yet been reached. The small jump in the imperfection-sensitivity curve at $\delta/t \cong 1.6$ in figure 7*a* for this case results from this transition in behaviour. In §7, it is found that non-axisymmetric bifurcation from the axisymmetric state prior to attainment of p_{max} does not occur for any of the cases presented in figure 7. Comparison of the results in figure 7*a* with those in figure 6 reveals that an imperfection in the shape of the classical mode does indeed reduce the buckling pressure slightly more than the comparable dimple imperfection at sufficiently small amplitudes, i.e. $\delta/t < 0.5$, but otherwise the dimple produces larger reductions.

Figure 7*b*, for shells with dimple imperfection size specified by $B = 1.5$, demonstrates again that there is essentially no dependence on R/t for thin shells as long as the imperfection width scales according to (6.2). A remarkable feature of these imperfection-sensitivity trends is the lower limit, or plateau, $p_{max}/p_C \simeq 0.2$, for buckling in the presence of imperfections with relatively large amplitudes, independent of R/t. This is another feature which might have surfaced decades ago had calculations at these larger imperfection amplitudes been performed. The plateau was first noted by Lee *et al.* [6] in a combined experimental and theoretical study of the buckling of clamped hemi-spherical shells. The plateau behaviour has important implications for identifying the knock-down factor for spherical shell buckling which will be discussed in the concluding remarks.

7. Non-axisymmetric bifurcation from the nonlinear axisymmetric state

The problem of non-axisymmetric bifurcation from the nonlinear axisymmetric solution is addressed to ascertain whether non-axisymmetric buckling solutions at p_{bif} exist prior to

attainment of $p_{\max}$ in the axisymmetric state. Such a non-axisymmetric bifurcation would indicate a lower buckling pressure than $p_{\max}$. The bifurcation solution is linearized about the nonlinear axisymmetric solution. Axial symmetry ensures a separated solution for the displacements in the form

$$(u_\omega, u_\theta, w) = R(\sin(m\omega)\,\bar{u}_\omega(\theta),\ \cos(m\omega)\,\bar{u}_\theta(\theta), \cos(m\omega)\,\bar{w}(\theta)), \tag{7.1}$$

where $m \geq 1$ is the unknown integer number of circumferential waves in the bifurcation mode. From (2.2) to (2.5) for the moderate rotation theory, the linearized rotation and strain measures have the form

$$\left.\begin{aligned} (\varphi_\omega, \varphi_\theta, \varphi_r) &= (\sin\omega\,\bar{\varphi}_\omega(\theta), \cos\omega\,\bar{\varphi}_\theta(\theta), \sin\omega\,\bar{\varphi}_r(\theta)), \\ (E_{\omega\omega}, E_{\theta\theta}, E_{\omega\theta}) &= (\cos\omega\,\bar{E}_{\omega\omega}(\theta), \cos\omega\,\bar{E}_{\theta\theta}(\theta), \sin\omega\,\bar{E}_{\omega\theta}(\theta)) \\ \text{and}\qquad (K_{\omega\omega}, K_{\theta\theta}, K_{\omega\theta}) &= \frac{1}{R}(\cos\omega\,\bar{K}_{\omega\omega}(\theta), \cos\omega\,\bar{K}_{\theta\theta}(\theta), \sin\omega\,\bar{K}_{\omega\theta}(\theta)), \end{aligned}\right\} \tag{7.2}$$

where the barred quantities are readily obtained in terms of $(\bar{u}_\omega(\theta), \bar{u}_\theta(\theta), \bar{w}(\theta))$, m and the rotation $\varphi_\theta^A(\theta)$ in the axisymmetric state (see appendix C).

Denote the quadratic functional of the non-axisymmetric displacements governing bifurcation from the axisymmetric state by $P_2(u_\omega, u_\theta, w)$. Attention is limited to axisymmetric solutions that are symmetric about the equator. This allows consideration of symmetric and antisymmetric bifurcations with respect to the equator with P_2 defined above the equator. The investigation of non-axisymmetric bifurcation occurs in the range of small rotations where the dead pressure is an excellent approximation to live pressure. As dead pressure is considerably simpler to implement, it will be used for the bifurcation analysis. When use is made of the separated form of the bifurcation mode listed above and the trivial integrations with respect to ω are carried out, one can show that P_2 can be reduced to the following dimensionless functional:

$$\left.\begin{aligned} \bar{P}_2(\bar{u}_\omega, \bar{u}_\theta, \bar{w}, p) = \frac{2(1-\nu^2)}{\pi R^2 E t} P_2 = \\ \int_0^{\pi/2} \left[(1-\nu)\bar{E}_{\alpha\beta}\bar{E}_{\alpha\beta} + \nu\bar{E}_{\gamma\gamma}^2 + \frac{1}{\hat{\alpha}}((1-\nu)\bar{K}_{\alpha\beta}\bar{K}_{\alpha\beta} + \nu\bar{K}_{\gamma\gamma}^2)\right]\cos\theta\,\mathrm{d}\theta \\ + \int_0^{\pi/2} [(E^A_{\omega\omega} + \nu E^A_{\theta\theta})(\bar{\varphi}_\omega^2 + \bar{\varphi}_r^2) + (E^A_{\theta\theta} + \nu E^A_{\omega\omega})(\bar{\varphi}_\theta^2 + \bar{\varphi}_r^2)]\cos\theta\,\mathrm{d}\theta, \end{aligned}\right\} \tag{7.3}$$

where $E^A_{\omega\omega}(\theta)$ and $E^A_{\theta\theta}(\theta)$ are the strains in the axisymmetric solution, $\hat{\alpha} = 12(R/t)^2$ and the dependence on p or w_{pole} arises through the axisymmetric solution. Symmetry at the equator requires $\bar{u}'_\omega = \bar{u}_\theta = \bar{w}' = \bar{w}''' = 0$ at $\theta = 0$, whereas antisymmetry requires $\bar{u}_\omega = \bar{u}'_\theta = \bar{w} = \bar{w}'' = 0$. For integers $m > 1$, conditions at the pole require $\bar{u}_\omega = \bar{u}'_\omega = \bar{u}_\theta = \bar{u}'_\theta = \bar{w} = \bar{w}' = 0$. The mode for $m = 1$ does not require $\bar{w}' = 0$ at the pole; it is an unknown, representing a possible tilt of the shell at the pole. For all the axisymmetric problems considered in this paper, w_{pole} is monotonically increasing and it has been used as the prescribed 'loading' parameter. For any non-zero set of admissible bifurcation displacements $(\bar{u}_\omega, \bar{u}_\theta, \bar{w})$, $\bar{P}_2 > 0$ for $w_{\text{pole}} < (w_{\text{pole}})_{\text{bif}}$ and there exist non-zero displacements such that $\bar{P}_2 < 0$ for $w_{\text{pole}} > (w_{\text{pole}})_{\text{bif}}$. The pole displacement at bifurcation, $(w_{\text{pole}})_{\text{bif}}$, is the lowest value of w_{pole}, considering all possible integers m for which an admissible non-zero mode $(\bar{u}_\omega, \bar{u}_\theta, \bar{w})$ exists with $\bar{P}_2 = 0$. The associated pressure at bifurcation is denoted by p_{bif}.

The numerical solution of the non-axisymmetric bifurcation problem employs cubic splines to represent each of the admissible displacements $(\bar{u}_\omega, \bar{u}_\theta, \bar{w})$ with nodal displacements as unknowns. With a_j, $j = 1, M$ denoting the vector of unknowns, (7.3) becomes

$$\bar{P}_2(\mathbf{a}, m, p) = \sum_{i=1}^{M}\sum_{j=1}^{M} A_{ij}a_i a_j, \tag{7.4}$$

where the symmetric matrix $\mathbf{A}$ is computed using numerical integration at each value of p, or equivalently at each value of pole displacement w_{pole}. For $w_{\text{pole}} < (w_{\text{pole}})_{\text{bif}}$, $\mathbf{A}$ is positive definite for all integers m; $(w_{\text{pole}})_{\text{bif}}$ is the lowest w_{pole} over all m such that $|\mathbf{A}| = 0$.

As reported in the earlier sections, no non-axisymmetric bifurcation was found for the axisymmetric post-buckling of the perfect shell for pole deflections as large as $w_{\text{pole}}/t = 10$ in figure 3 once the axisymmetric bifurcation mode had been established. Furthermore, no non-axisymmetric bifurcation was found for the axisymmetric solutions associated with the dimple imperfection prior to attainment of the maximum pressure in the axisymmetric state. In fact, for all cases investigated for the dimple imperfection, non-axisymmetric bifurcation from the axisymmetric state did not occur even well past the maximum pressure. While it is not possible to claim that non-axisymmetric bifurcation never occurs for axisymmetric dimple-like imperfections, it appears from the examples investigated here that the axisymmetric deformation becomes 'locked in' and resistant to non-axisymmetric deformation. As noted in §5, for imperfections in the shape of the classical mode, the only instance where bifurcation from the axisymmetric state was observed was for larger imperfections ($\delta/t > 0.9$) in the range where the maximum pressure increases with increasing imperfection amplitude. Although the imperfection in the shape of the classical mode has potency at small amplitudes, it is not nearly as damaging at larger amplitudes as the dimple imperfection and it is less realistic.

The study summarized thus far has established that an axisymmetric dimple imperfection is likely to produce an axisymmetric buckling response when the spherical shell is subject to uniform pressure. Imperfection amplitudes slightly larger than a shell thickness reduce the buckling pressure to $p_{\max}/p_C \cong 0.2$. We now show that axisymmetric imperfections at the equator, the so-called beltline imperfections, can produce comparable buckling pressure reductions. For these imperfections, buckling is associated with non-axisymmetric bifurcation from the axisymmetric state.

The axisymmetric beltline imperfection is symmetric with respect to the equator and specified by

$$w_I(\theta) = \begin{cases} -\delta \cos\left(\dfrac{2\pi R\theta}{\ell_C}\right), & 0 \le |\theta| \le \theta_A, \\ \delta p^{(5)}(\theta), & \theta_A \le |\theta| \le \theta_B, \\ 0, & \theta_B \le |\theta| \le \frac{\pi}{2}. \end{cases} \tag{7.5}$$

It is plotted in figure 8*a* for the specific choices, $\theta_A = 59.41°$ and $\theta_B = 74.71°$, used in this paper. Here, $\ell_C = 2\pi R/q_0$ is the critical axisymmetric wavelength ℓ_θ given by (3.9) with $\ell_\omega \to \infty$, and $p^{(5)}(\theta)$ is the fifth-order polynomial chosen such that w_I and its first and second derivatives are continuous at θ_A and θ_B. The region in the vicinity of the pole is imperfection free and the maximum imperfection amplitude is δ attained in the vicinity of the equator.

The nonlinear axisymmetric solution for the beltline imperfection (7.5) does not display a maximum until p becomes almost p_C even for relatively large imperfection amplitudes. Thus, if one restricted consideration to axisymmetric behaviour, one would have to conclude that the beltline imperfection does not give rise to buckling imperfection sensitivity. The conclusion is entirely different, however, when non-axisymmetric bifurcation from the axisymmetric solution is considered. Results of the non-axisymmetric bifurcation study for a shell with $R/t = 100$ and $\nu = 0.3$ are shown in figure 8*b*, where the normalized bifurcation pressure, p_{bif}/p_C, is plotted versus the normalized imperfection amplitude, δ/t. In this plot, the number of circumferential waves, m, associated with the bifurcation mode is shown. The slight rise seen in the bifurcation pressure in figure 8*b* as δ/t approaches 2 has been evaluated carefully—it is not numerical error. For $\delta/t > 0$, as in figure 8*b*, the lowest bifurcation eigenvalue is associated with a mode $(\bar{u}_\omega, \bar{u}_\theta, \bar{w})$ which is symmetric with respect to the equator, although the analysis assuming an antisymmetric mode generates only slightly larger eigenvalues. For $\delta/t < 0$, the critical mode is antisymmetric and the imperfection-sensitivity curve is essentially identical to that in figure 8*b*. The explanation of the underlying interaction of the non-axisymmetric mode with the membrane stresses generated by the nonlinear axisymmetric solution is similar to that provided in the study

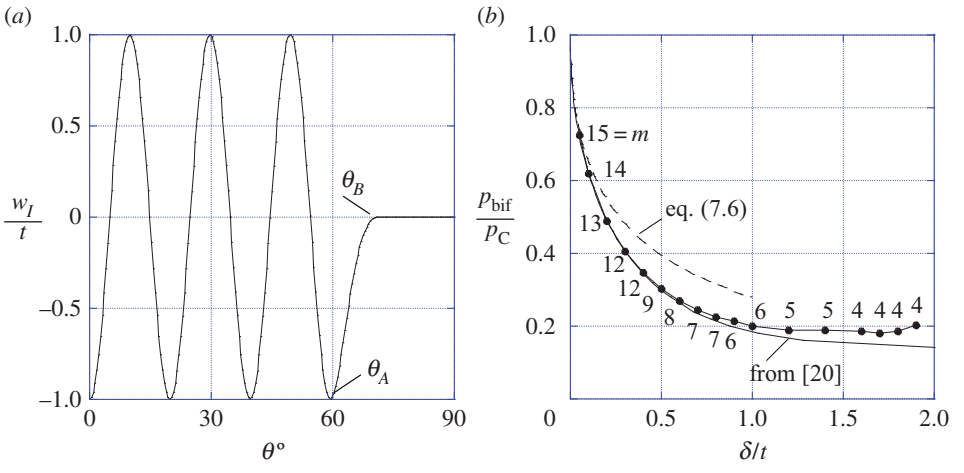

Figure 8. Non-axisymmetric bifurcation from the axisymmetric state for axisymmetric equatorial, 'beltline', imperfections for a spherical shell with $R/t = 100$ and $\nu = 0.3$. The imperfection, specified by (7.5), is plotted in (*a*) for $\delta/t = 1$, with $\theta_A = 59.41°$ and $\theta_B = 74.71°$. The pressure at bifurcation computed for the full sphere using moderate rotation theory is plotted in (*b*) as the curve which displays the number of circumferential waves m associated with the lowest bifurcation pressure. Included in (*b*) are two results from [20] for the same imperfection based on an analysis of a shallow equatorial section of the shell. The upper dashed curve is the asymptotic imperfection-sensitivity formula (7.6) and the lower solid line curve is a more accurate analytical result not limited to small imperfections. (Online version in colour.)

of the effect of axisymmetric imperfections on the non-axisymmetric bifurcation of cylindrical shells under axial compression [26].

Except for very small imperfections in the shape of the classical mode, the beltline imperfection produces somewhat larger buckling pressure reductions than the other two shapes considered for imperfection amplitudes with $\delta/t \leq 1$. For larger imperfection amplitudes, the beltline and dimple imperfections both give rise to buckling pressure reductions that level out at $p/p_C \cong 0.2$.

Included in figure 8*b* are results from two analyses taken from Hutchinson [20] for a sinusoidal imperfection with precisely the same form as (7.5) near the equator. The two analyses employed DMV theory but did not consider a full spherical shell. Instead, the analyses exploited the short wavelengths of the modes in the vicinity of the equator and considered periodic mode interaction in a shallow section of the shell. The dashed curve in figure 8 is the relation

$$\left(1 - \frac{p_{bif}}{p_C}\right)^2 = \frac{9\sqrt{3(1-\nu^2)}}{8}\frac{\delta}{t}\frac{p_{bif}}{p_C}, \tag{7.6}$$

based on a Koiter-type asymptotic analysis. The second result, plotted as the lowest solid curve in figure 8*b*, agrees with (7.6) asymptotically for small δ/t but is not restricted to small imperfections, although it is approximate being based on the shallow analysis. This second curve is a slightly more complicated analytic result taken from the appendix of [20]. These two results for p_{bif}/p_C do not depend on R/t, and we strongly expect that the results from the full shell analysis in figure 8 will be essentially the same for all larger R/t. This has indeed been verified with $R/t = 200$ for selected values of δ/t over the range shown in figure 8*b*. For these additional calculations, the imperfection wavelength and the angles defining the transition to the imperfection-free pole are changed consistent with the dependence on R/t in (7.5)

The imperfection-sensitivity prediction based on the numerical analysis of moderate rotation theory for the full sphere in figure 8*b* is remarkably close to the analytical prediction given in the appendix of [20] for $\delta/t \leq 1$. This agreement provides convincing evidence that Koiter [1] is not correct in his assertion that by ignoring boundary conditions the shallow periodic analysis produces an overly large pressure reduction. Koiter [1] modified the shallow analysis by

modulating the periodic modes with an exponential function such that the modes decay to zero outside the interaction region. His modification of the shallow analysis notably under-predicts the buckling load reductions for the full sphere shown in figure 8. It can also be mentioned that the one instance in the present work where we have found some divergence between calculations based on DMV theory and the moderate rotation theory is in the range of larger imperfections in figure 8*b*. At these larger imperfection levels, the bifurcation mode has a relatively low circumferential wavenumber, $m = 4$, and thus it is not surprising that the shallow deformation assumption underlying the approximations in DMV theory begins to break down. However, even in the range $1.5 < \delta/t < 2$, the deviation of $p_{\mathrm{bif}}/p_{\mathrm{C}}$ from DMV theory compared with the prediction of moderate rotation theory is not more than 5%.

8. Conclusion

The major findings of this study are as follows:

(i) For the perfect spherical shell undergoing axisymmetric deformation, localization of the non-uniform buckling deflection at the pole occurs almost immediately after the onset of buckling. The localized mode bears little similarity to the classical buckling mode. This is the reason that a post-bifurcation expansion with the classical mode as the dominant term has such a small range of validity. Once initiated, the axisymmetric solution is resistant to non-axisymmetric bifurcations.

(ii) Axisymmetric dimple imperfections located at the pole with amplitudes of one shell thickness reduce the buckling pressure to approximately 20% of the buckling pressure of the perfect shell, reaching a plateau with no further reduction produced by larger imperfection amplitudes. Non-axisymmetric bifurcation from the axisymmetric solution does not occur for these imperfection shapes prior to attainment of the maximum pressure.

(iii) Axisymmetric sinusoidal imperfections in the vicinity of the equator, the so-called beltline imperfections, produce reductions to the buckling pressure that are somewhat larger than those caused by dimple imperfections but approach a similar plateau limit. Buckling occurs as a result of non-axisymmetric bifurcation from the axisymmetric state.

(iv) Critical imperfection widths are proportional to $\sqrt{Rt}$ and, for imperfection shapes that scale accordingly, the imperfection-sensitivity curves obtained here are essentially independent of R/t. Moreover, the buckling pressures are attained in the range of relatively small deflections such that either moderate rotation theory or DMV theory is accurate with virtually no distinction between live and dead pressure.

From a practical standpoint, the most important discovery for spherical shell buckling is the levelling out of the imperfection-sensitivity curve on the plateau at roughly 20% of the buckling pressure of the perfect shell. The plateau is also observed for the beltline imperfections. More extensive analysis of the plateau for a wider range of dimple imperfection widths has been presented by Lee *et al*. [6] for hemi-spherical shells clamped at the equator. These alternative boundary conditions produce virtually no change in the imperfection-sensitivity curves from those obtained here. It is found that, for an extended range of imperfection widths, the plateau lies between 15% and 20% of the classical pressure. It is tempting to associate the buckling pressure reduction on the plateau with the knock-down factor of 20% widely used for design against elastic buckling of thin spherical shells. The plateau is associated with a wide range of realistic dimple widths. More numerical and experimental work will be required to establish the robustness of the plateau for other imperfection shapes and types, especially for non-axisymmetic imperfections. Nevertheless, new experimental data for the elastic buckling of spherical shells obtained by Lee *et al*. [6] support the existence of a plateau in the buckling pressure for larger imperfections. In addition, trends in the experimental data for buckling of spherical shells collected in [27] give further hope that the plateau may be relevant to the apparent lower limit of the buckling data.

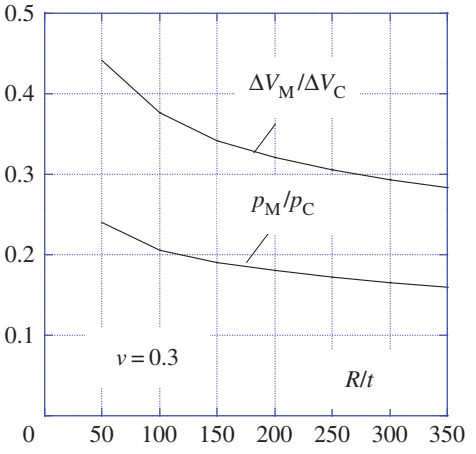

Figure 9. Prescribed volume change, $\Delta V = \Delta V_M$, and post-buckling pressure of the perfect spherical shell at the Maxwell condition where the elastic energies in the buckled and unbuckled states are equal. (Online version in colour.)

In addition to non-axisymmetric imperfections, this study leaves several other aspects unexplored. These include questions of whether the non-axisymmetric bifurcation from the axisymmetric state for the beltline imperfections is stable or unstable, and the relevance of the minimum pressure in the post-buckling state of the perfect shell under prescribed volume change or other such criteria. Even if the bifurcation from the axisymmetric state is stable such that the shell can carry pressure above p_{bif}, it is likely that the additional pressure-carrying capacity will be quite small and that significant non-axisymmetric buckling deflections can be expected after p_{bif} is attained. Thus, even if the bifurcation is stable, the bifurcation pressure is almost certainly a reasonable measure of the effective buckling pressure. In a related study [28] of the stability of non-axisymmetric bifurcation of a cylindrical shell with an axisymmetric imperfection under axial load P, it was found that the bifurcation is unstable for imperfection amplitudes such that P_{bif}/P_C was greater than about 20% and stable when P_{bif}/P_C was less than 20%, where P_C is the buckling load of the perfect cylinder.

Figure 2 makes it fairly obvious that the minimum pressure of the perfect spherical shell in the post-buckling state does not have any direct relevance to the buckling pressure of imperfect shells. It is also questionable whether, even under prescribed volume change ΔV, either DMV theory or moderate rotation theory can be used to accurately compute the minimum pressure. Note from figure 5*b* that for a perfect shell with $R/t = 103.5$ the post-buckling pressure for ΔV prescribed to be ΔV_C is $p/p_C \cong 0.13$ occurring for w_{pole}/t considerably larger than 10. This prediction may lie outside the range for which moderate rotation theory is accurate.

It is possible to accurately compute the post-buckling pressure associated with the Maxwell condition for prescribed volume change for the perfect shell using moderate rotation theory, and this condition may be more relevant than the minimum post-buckling pressure. The Maxwell volume change is defined as the prescribed volume change ΔV_M for which the elastic energy in the uniform state equals the elastic energy in the post-buckled state, with the elastic energy given by Ψ in (2.12) without the pressure contribution. The associated pressure in the post-buckled state is denoted by p_M. Accurate results for ΔV_M and p_M as a function of R/t are plotted in figure 9. Friedrichs [29] and Tsien [30] originally proposed the Maxwell pressure of the perfect shell p_M as a possible criterion for the lower limit of experimental buckling pressures but this idea seems never to have been seriously pursued until recently [12,13]. The trend line for p_M/p_C in figure 9 suggests that this idea may have some merit. It will be further pursued in a subsequent paper.

Data accessibility. All data are contained within the published paper.
Competing interests. I declare I have no competing interests.

Funding. I received no funding for this study.
Acknowledgement. The author is indebted to stimulating interactions from two sources. One is Pedro Reis and his group at MIT working on spherical shell buckling: Francisco Jiménez, Anna Lee and Joel Marthelot. The other is Michael (J.M.T.) Thompson, an early contributor to spherical shell buckling, who is now approaching the subject within the framework of nonlinear dynamics.

Appendix A. Specification of the ODE system for axisymmetric deformations

The moderate rotation equations are specialized to axisymmetric deformations such that u_θ, w and w_I are functions of θ with $u_\omega = 0$. Solutions symmetric about the equator can be analysed on $(0 \le \theta \le \pi/2)$. Dimensionless displacements are defined as $U = u_\theta/R$, $W = w/R$ and $W_\mathrm{I} = w_\mathrm{I}/R$. Let $\mathrm{d}()/\mathrm{d}\theta = ()'$. Then, with

$$\varphi_\theta = -W' + U \quad \text{and} \quad e \equiv e_{\theta\theta} = W + U', \tag{A 1}$$

the non-zero strains are

$$\left.\begin{aligned} E_{\omega\omega} &= W - U\tan\theta, \\ E_{\theta\theta} &= e + \frac{1}{2}{\varphi_\theta}^2 - W_I'\varphi_\theta, \\ K_{\omega\omega} &= -\frac{1}{R}\tan\theta\,\varphi_\theta \\ \text{and} \qquad K_{\theta\theta} &= \frac{1}{R}\varphi_\theta'. \end{aligned}\right\} \tag{A 2}$$

Equilibrium equations are generated either by requiring $\delta\Psi = 0$ for all admissible variations (δU, δW) or, equivalently, by enforcing the principle of virtual work. The two equilibrium equations for dead pressure are

$$\bar{m}_\theta'' + (\tan\theta\,\bar{m}_\omega)' - \frac{1}{(1-\nu^2)}(\hat{n}_\theta + \hat{n}_\omega + (\hat{n}_\theta(\varphi_\theta - {W_\mathrm{I}}'))') + \bar{p} = 0 \tag{A 3}$$

and

$$\bar{m}_\theta' + \tan\theta\,\bar{m}_\omega + \frac{1}{(1-\nu^2)}(\hat{n}_\theta' + \tan\theta\,\hat{n}_\omega - \hat{n}_\theta(\varphi_\theta - {W_I}')) = 0, \tag{A 4}$$

where

$$\left.\begin{aligned} (\hat{n}_\omega, \hat{n}_\theta) &= \frac{\hat{\alpha}}{Et}\cos\theta(N_{\omega\omega}, N_{\theta\theta}), \\ (\bar{m}_\omega, \bar{m}_\theta) &= \frac{R}{D}\cos\theta(M_{\omega\omega}, M_{\theta\theta}) \\ \text{and} \qquad \bar{p} &= \frac{R^3}{D}\cos\theta\,p, \end{aligned}\right\} \tag{A 5}$$

and $\hat{\alpha} = 12\,(R/t)^2$. The additional terms for live pressure have not been listed since they are lengthy, but they are readily generated.

The equilibrium equations can be expressed through the constitutive equations and the strain–displacement relations in terms of U and W or, equivalently, in terms of φ_θ and W with $U = W' + \varphi_\theta$. The most highly differentiated terms are φ_θ''' and W''' such that this is a sixth-order, nonlinear ODE system. In all the problems considered in the paper, the axisymmetric behaviour is such that the inward deflection at the pole, $-W(\pi/2)$, increases monotonically, while the pressure, $\tilde{p} = R^3 p/D$, increases in the early stages and then usually attains a limit point after which it decreases. For this reason, it is effective to treat $\tilde{p}$ as an unknown, to introduce an extra ODE, $\mathrm{d}\tilde{p}/\mathrm{d}\theta = 0$, and

to prescribe $-W(\pi/2)$ as the 'load parameter'. This augmented system can be reduced to seven first-order ODEs in the standard form

$$\left.\begin{aligned} \frac{\mathrm{d}\boldsymbol{y}}{\mathrm{d}\boldsymbol{\theta}} &= \boldsymbol{f}(\theta, \boldsymbol{y}), \\ \text{where} \quad \boldsymbol{y} &= (\varphi_\theta'', \varphi_\theta', \varphi_\theta, W'', W', W, \tilde{p}). \end{aligned}\right\} \tag{A 6}$$

When used in conjunction with a modern nonlinear ODE solver, this formulation provides highly accurate results. In particular, the buckling pressure, i.e. the maximum pressure attained at the limit point, can be accurately calculated. We have used the ODE solver routine DBVPFD in IMSL,[1] which incorporates Newton iteration to satisfy the nonlinear equations and automatic mesh refinement to meet accuracy tolerances. As already noted, the inward pole deflection serves as the loading parameter and it is increased in steps using a converged solution at one step as the starting guess for the next step. The solution process is fast and robust. The results presented as p/p_C versus w_{pole}/t or $\Delta V/\Delta V_C$, which have been presented in the various figures, are generated to an accuracy of three significant figures.

The components of $\boldsymbol{f}$ in (A 5) are given below.

$$\begin{aligned} \varphi_\theta''' = f_1 = \frac{1}{\cos\theta}\Bigg[&(2+\nu)\sin\theta\,\varphi_\theta'' + (1+2\nu)\cos\theta\,\varphi_\theta' - \nu\sin\theta\,\varphi_\theta - \tan\theta\,\bar{m}_\omega' - \frac{\bar{m}_\omega}{\cos^2\theta} \\ &+ \hat{n}_\theta(1+\varphi_\theta' - W_I'') + \hat{n}_\omega + \hat{n}_\theta'(\varphi_\theta - W_I') + \bar{p}\Bigg], \\ f_2 = \varphi_\theta'', \quad f_3 = \varphi_\theta', \\ W''' = f_4 = -\varphi_\theta'' - W' - \varphi_\theta'(\varphi_\theta - W_I') + \varphi_\theta W_I'' + \tan\theta(E_{\theta\theta} + \nu E_{\omega\omega}) \\ + \frac{1}{\hat{\alpha}\cos\theta}[\hat{n}_\theta(\varphi_\theta - W_I') - \tan\theta(\hat{n}_\omega + \bar{m}_\omega) - \bar{m}_\theta'] \end{aligned}$$

and $$f_5 = W'', \quad f_6 = W', \quad f_7 = 0.$$

In the above, $\bar{m}_\omega = -\sin\theta\,\varphi_\theta + \nu\cos\theta\,\varphi_\theta'$, $\bar{m}_\omega' = \nu\cos\theta\,\varphi_\theta'' - (1+\nu)\sin\theta\,\varphi_\theta' - \cos\theta\,\varphi_\theta$, $\bar{m}_\theta' = \cos\theta(\varphi_\theta'' - \nu\varphi_\theta) - (1+\nu)\sin\theta\,\varphi_\theta'$, $\hat{n}_\omega = \hat{\alpha}\cos\theta(E_{\omega\omega} + \nu E_{\theta\theta})$ and $\hat{n}_\theta = \hat{\alpha}\cos\theta(E_{\theta\theta} + \nu E_{\omega\omega})$, where $E_{\omega\omega}$ and $E_{\theta\theta}$ are given by (A 1) and (A 2), respectively, using $U = \varphi_\theta + W'$. The derivative, $\hat{n}_\theta'$, is directly computed in terms of φ_θ and W and their derivatives.

At the equator ($\theta = 0$), symmetry requires $\varphi_\theta = 0$, $\varphi_\theta'' = 0$ and $W' = 0$. The functions φ_θ and W are analytic at the pole, with φ_θ being odd and W even about the pole such that $\varphi_\theta'' = 0$, $\varphi_\theta = 0$ and $W' = 0$ at $\theta = \pi/2$. At the pole, $f_2 = 0, f_3 = \varphi_\theta', f_4 = 0, f_5 = W'', f_6 = 0$ and $f_7 = 0$. A somewhat lengthy expansion about the pole provides the following expression for φ_θ''' at $\theta = \pi/2$:

$$f_1 = \tfrac{3}{8}\left[2(-\tfrac{1}{3} + \nu)\varphi_\theta' + 2\hat{\alpha}(1+\nu)(\varphi_\theta' + W'' + W)(1 + \varphi_\theta' - W_I'') + \tilde{p}\right]. \tag{A 7}$$

Again, the additional terms for live pressure have not been listed, because they are lengthy but they are readily generated.

Appendix B. Solution method for axisymmetric deformations with the exact formulation

The numerical methods for solving the axisymmetric problems in §4 based on the shell formulation employing exact measures of the middle surface strains and curvature changes and those for solving the non-axisymmetric bifurcation problem in §7 both employ splines to represent the unknown fields with nodal values serving as unknowns. For the exact axisymmetric formulation in §2c, $u(\theta)$ and $w'(\theta)$ are each represented by cubic splines and their values at the nodes $\theta_i = (i-1)\pi/(2(N-1))$ for $i = 1, N$ serve as unknowns. As both $u(\theta)$ and $w'(\theta)$ are odd about the pole and the equator, it follows that they vanish at the pole and the equator. With

[1]IMSL (1994). Numerical analysis software copyrighted by Visual Numerics, Inc., USA.

$w(\pi/2)$ as the one additional unknown, $w(\theta)$ is given by $w(\theta) = w(\pi/2) - \int_\theta^{\pi/2} w'(\tilde{\theta})\,\mathrm{d}\tilde{\theta}$, which is integrated using the splines for $w'(\theta)$. This representation has continuous first and second derivatives of $u(\theta)$ and continuous first, second and third derivatives of $w(\theta)$. There are $M = 2N - 3$ unknowns, (u_i, w_i'), $i = 2, N-1$ and $w(\pi/2)$, denoted by the vector $\mathbf{a}$. For any $\mathbf{a}$, the energy functional $\Psi(\mathbf{a}, p)$ in (2.12) is evaluated by numerical integration. The attraction of this method is that it is exceptionally straightforward and simple to program. The numerical evaluation of Ψ is achieved with high accuracy using established integration formulae. It should be mentioned that an alternative method would be to follow through the steps to generate a system of ODEs similar to that described for the moderate rotation theory in appendix A. This alternative is feasible, but the algebraic work is enormous, as is the programing due to the lengthy nature of the bending strains and the more complicated stretching strain expressions.

The admissible set of displacements represented by $\mathbf{a}$ must render Ψ stationary, i.e. $\partial\Psi(\mathbf{a}, p)/\partial a_j = 0$, $j = 1, M$. With $(\mathbf{a}^0, p^0)$ as an estimated solution to the stationarity equations, the linearized equations for estimating improvements, $\Delta\mathbf{a}$ and Δp, are

$$\frac{\partial^2\Psi(\mathbf{a}^0, p^0)}{\partial a_j \partial a_k}\Delta a_k + \frac{\partial^2\Psi(\mathbf{a}^0, p^0)}{\partial a_j \partial p}\Delta p = -\frac{\partial\Psi(\mathbf{a}^0, p^0)}{\partial a_j}, \quad j = 1, M \tag{B 1}$$

with summation on k. This same set of equations can be used if $\Delta w(\pi/2)$ is the prescribed change and Δp is unknown. The partial derivatives in these equations are computed numerically. The solutions generated in figures 2 and 3 were obtained by prescribing an increment of pole deflection $\Delta w(\pi/2)$ and computing the remaining unknown increments $\Delta\mathbf{a}$ and Δp. Newton iteration using (B 1) with $\Delta w(\pi/2) = 0$ is also employed to converge at each step. The method is efficient and effective as long as R/t is not too large. The number of splines N scales with $\sqrt{R/t}$. Accurate solutions for $R/t = 50$ are obtained with $N = 30$. In contrast with the ODE method, a drawback of this method is that it becomes difficult to obtain convergence for large R/t.

Appendix C. Solution to the non-axisymmetric bifurcation eigenvalue problem

The expressions for the rotation and strain quantities in terms of $(\bar{u}_\omega(\theta), \bar{u}_\theta(\theta), \bar{w}(\theta))$ are

$$\varphi_\omega = \sin m\omega\,\bar{\varphi}_\omega = \sin m\omega\left(\frac{m}{\cos\theta}\bar{w} + \bar{u}_\omega\right),$$

$$\varphi_\theta = \cos m\omega\,\bar{\varphi}_\theta = \cos m\omega\,(-\bar{w}' + \bar{u}_\theta),$$

$$\varphi_r = \sin m\omega\,\bar{\varphi}_r = \sin m\omega\,\frac{1}{2}\left(-\frac{m}{\cos\theta}\bar{u}_\theta + \tan\theta\,\bar{u}_\omega - \bar{u}_\omega'\right),$$

$$E_{\omega\omega} = \cos m\omega\;\bar{E}_{\omega\omega} = \cos m\omega\left(\frac{m}{\cos\theta}\bar{u}_\omega - \tan\theta\,\bar{u}_\theta + \bar{w}\right),$$

$$E_{\theta\theta} = \cos m\omega\;\bar{E}_{\theta\theta} = \cos m\omega\,(\bar{u}_\theta' + \bar{w} + \varphi_\theta^A\bar{\varphi}_\theta),$$

$$E_{\omega\theta} = \sin m\omega\;\bar{E}_{\omega\theta} = \sin m\omega\,\frac{1}{2}\left(\bar{u}_\omega' - \frac{m}{\cos\theta}\bar{u}_\theta + \tan\theta\,\bar{u}_\omega + \varphi_\theta^A\bar{\varphi}_\omega\right),$$

$$K_{\omega\omega} = \cos m\omega\;\frac{1}{R}\bar{K}_{\omega\omega} = \cos m\omega\,\frac{1}{R}\left(\frac{m}{\cos\theta}\bar{\varphi}_\omega - \tan\theta\,\bar{\varphi}_\theta\right),$$

$$K_{\theta\theta} = \cos m\omega\;\frac{1}{R}\bar{K}_{\theta\theta} = \cos m\omega\,\frac{1}{R}(\bar{\varphi}_\theta')$$

and

$$K_{\omega\theta} = \sin m\omega\;\frac{1}{R}\bar{K}_{\omega\theta} = \sin m\omega\,\frac{1}{2R}\left(\bar{\varphi}_\omega' + \tan\theta\,\bar{\varphi}_\omega - \frac{m}{\cos\theta}\bar{\varphi}_\theta\right),$$

where $\varphi_\theta^A(\theta)$ is $\varphi_\theta(\theta)$ from the axisymmetric solution and $()' = \mathrm{d}()/\mathrm{d}\theta$.

As described in §7, cubic splines are used to represent $(\bar{u}_\omega(\theta), \bar{u}_\theta(\theta), \bar{w}(\theta))$ in much the same way as described in appendix B for the axisymmetric problems. In addition to involving $\bar{u}_\omega$, the method for the non-axisymmetric bifurcation represents $\bar{w}$, not $\bar{w}'$, using cubic splines. Thus, only continuity of $\bar{w}$ and its first two derivatives is ensured. Otherwise, the method is as described

in §7. The search for the lowest eigenvalue requires systematic consideration of all integers m and both symmetric and antisymmetric eigenmodes at each value of p or, equivalently, of w_{pole}. The number of splines N needed to represent each of the three unknown displacements scales with $\sqrt{R/t}$, and $N \cong 2\sqrt{R/t}$ gave accurate results.

References

1. Koiter WT. 1969 The nonlinear buckling behavior of a complete spherical shell under uniform external pressure, Parts I, II, III & IV. *Proc. Kon. Ned. Ak. Wet.* **B72**, 40–123.
2. von Karman T, Tsien HS. 1939 The buckling of spherical shells by external pressure. *J. Aero. Sci.* **7**, 43–50. (doi:10.2514/8.1019)
3. Koiter WT. 1945 On the stability of elastic equilibrium. Dissertation, Delft, The Netherlands. An English translation is available in 1967. *Tech. Trans. F* **10**, 833.
4. Thompson JMT. 1964 The rotationally-symmetric branching behavior of a complete spherical shell. *Proc. Kon. Ned. Ak. Wet.* **B67**, 295–311.
5. Lee A, Brun PT, Marthelot J, Balestra G, Gallaire F, Reis PM. 2016 Fabrication of slender elastic shells by the coating of curved surfaces. *Nat. Commun.* **7**, 11155. (doi:10.1038/ncomms11155)
6. Lee A, Marthelot J, Jimenez FL, Hutchinson JW, Reis PM. 2016 The geometric role of precisely engineered imperfections on the critical buckling load of spherical elastic shells. *J. Appl. Mech.* **83**, 111005. (doi:10.1115/1.4034431)
7. Vaziri A, Mahadevan L. 2008 Localized and extended deformations of elastic shells. *Proc. Natl Acad. Sci. USA* **105**, 7913. (doi:10.1073/pnas.0707364105)
8. Pamplona DC, Calladine CR. 1993 The mechanics of axially symmetric liposomes. *J. Biomech. Eng.* **115**, 149–159. (doi:10.1115/1.2894115)
9. Katifori E, Alben S, Cerda E, Nelson DR, Dumais J. 2010 Foldable structures and the natural design of pollen grains. *Proc. Natl Acad. Sci. USA* **107**, 7635–7639. (doi:10.1073/pnas.0911223107)
10. Datta SS, Kim SH, Paulose J, Abbaspourrad A, Nelson DR, Weitz DA. 2012 Delayed buckling and guided folding of inhomogeneous capsules. *Phys. Rev. Lett.* **109**, 134302. (doi:10.1103/PhysRevLett.109.134302)
11. Paulose J, Nelson DR. 2013 Buckling pathways in spherical shells with soft spots. *Soft Matter.* **9**, 8227–8245. (doi:10.1039/c3sm50719j)
12. Thompson JMT, van der Heijden GHM. 2014 Quantified 'shock-sensitivity' above the Maxwell load. *Int. J. Bif. Chaos* **24**, 1430009. (doi:10.1142/S0218127414300092)
13. Thompson JMT, Sieber J. 2016 Shock-sensitivity in shell-like structures: with simulations of spherical shell buckling. *Int. J. Bif. Chaos* **26**, 1630003. (doi:10.1142/S0218127416300032)
14. Horak J, Lord DJ, Peletier MA. 2006 Cylinder buckling: the mountain pass as an organizing center. *SIAM J. Appl. Math.* **66**, 1793–1824. (doi:10.1137/050635778)
15. Sanders JL. 1963 Nonlinear shell theories for thin shells. *Quart. Appl. Math.* **21**, 21–36.
16. Koiter WT. 1966 On the nonlinear theory of thin elastic shells. *Proc. Kon. Ned. Ak. Wet. B* **69**, 1–54.
17. Koiter WT. 1967 General equations of elastic stability for thin shells. In *Proceedings—Symposium on the Theory of Shells to Honor Lloyd Hamilton Donnell* (ed. D Muster), pp. 187–227. Houston, TX: University of Houston.
18. Budiansky B. 1968 Notes on nonlinear shell theory. *J. Appl. Mech.* **35**, 393–401. (doi:10.1115/1.3601208)
19. van der Neut A. 1932 De elastische stabiliteit van den dunwandigen bo. Dissertation, Delft, The Netherlands.
20. Hutchinson JW. 1967 Imperfection-sensitivity of externally pressurized spherical shells. *J. Appl. Mech.* **34**, 49–55. (doi:10.1115/1.3607667)
21. Evkin A, Kolesnikov M, Prikazchikov DA. 2016 Buckling of a spherical shell under external pressure and inward concentrated load: asymptotic solution. *Math. Mech. Solids* **1**, 1–13. (doi:10.1177/1081286516635872)
22. Koga T, Hoff NJ. 1969 The axisymmetric buckling of initially imperfect spherical shells. *Int. J. Solids Struct.* **5**, 679–697. (doi:10.1016/0020-7683(69)90088-2)
23. Bushnell D. 1967 Nonlinear axisymmetric behavior of shells of revolution. *AIAA J.* **5**, 432–439. (doi:10.2514/3.3998)

24. Bushnell D. 1989 *Computerized buckling analysis of shells*. Dordrecht, The Netherlands: Kluwer Academic Publishers.
25. Bushnell D. 1965 Some problems in the theory of thin shells. PhD Dissertation, Department of Aeronautics and Astronautics, Stanford University, Stanford, CA, USA.
26. Koiter WT. 1963 The effect of axisymmetric imperfections on the buckling of cylindrical shells under axial compression. *Proc. Kon. Ned. Ak. Wet.* **B66**, 265–279.
27. Wunderlich W, Albertin U. 2002 Buckling behavior of imperfect spherical shells. *Int. J. Nonlin. Mech.* **37**, 589–604. (doi:10.1016/S0020-7462(01)00086-5)
28. Budiansky B, Hutchinson JW. 1972 Buckling of circular cylindrical shells under axial compression. In *Contributions to the theory of aircraft structures*, pp. 239–260. Rotterdam, The Netherlands: Delft University Press, Nijgh-Wolters-Noordhoff University Publishers.
29. Friedrichs KO. 1941 On the minimum buckling load of spherical shells. In *Theodore Von Kármán, Anniversary Volume: Contributions to Applied Mechanics and Related Subjects by the Friends of Theodore Von Kármán on His Sixtieth Birthday*, pp. 258–272. Pasadena, CA: California Institute of Technology.
30. Tsien HS. 1947 Lower buckling load in the non-linear bucking theory for thin shells. *Quart. Appl. Math.* **5**, 236–239.